

Supplementary Materials for
A nearly terrestrial D/H for comet 67P/Churyumov-Gerasimenko

Kathleen E. Mandt *et al.*

Corresponding author: Kathleen E. Mandt, kathleen.mandt@nasa.gov

Sci. Adv. **10**, eadp2191 (2024)
DOI: 10.1126/sciadv.adp2191

The PDF file includes:

Supplementary Text
Figs. S1 to S7
Tables S1 to S9
Legend for data S1
References

Other Supplementary Material for this manuscript includes the following:

Data S1

Supplementary Text

Water isotope measurements throughout the solar system

Tables S1, S2, and S3 list the isotopic ratios illustrated in Figure 1, the molecule in which the ratio is measured, and the source of the measurement. These observations are used to constrain the hydrogen and oxygen isotope ratios in the PSN, and to determine how the terrestrial planets obtained water and other volatile materials. The measurement for D/H in the PSN represents H₂, the main species in the nebula. This value is based on D/H in Jupiter's atmosphere, which obtained the vast majority of its H₂ from the PSN when Jupiter formed (3). Deuterium is converted in the Sun to ³He, reducing D/H in the Sun over time compared to the value that was present in the PSN. The oxygen isotopes in the PSN were determined based on a review of solar composition (53).

Saturn (54) has a lower D/H than Jupiter, but the uncertainty on this measurement is large and does not exclude a value similar to Jupiter's. What is needed is to measure D/H with an atmospheric probe, similar to the measurements made at Jupiter (55). The D/H in Neptune and Uranus (56) is enhanced compared to Jupiter and Saturn as the result of water ice and other volatiles enriched in deuterium forming the building blocks for these planets. As with Saturn, an atmospheric probe is needed to reduce the uncertainty on these measurements (55). Oxygen isotope measurements in the giant planets are limited to a single ¹⁶O/¹⁸O measurement for Jupiter (57) that has too large of error bars for any reasonable conclusion to be made about the formation of the planet.

Of the solid bodies that can serve as time capsules for conditions in the PSN, chondrites formed closest to the Sun. They are thought to have originated as asteroids that once had some water ice. The D/H for this ice is preserved in hydrated silicates (58). The oxygen isotopes for water are estimated based on modeling of isotopic fractionation in chondrites (59,60). Most chondrites have terrestrial D/H, with the exception CR and LL chondrites which are ~2-3 times greater than terrestrial. All chondrites have oxygen isotope ratios very close to the terrestrial value.

The water ice that formed the building blocks of Saturn's moons is thought to be from the same region where Saturn formed. The D/H on the surface of several moons has been measured and found to be enriched by up to 3 x terrestrial with error bars that overlap terrestrial values (42). This is in agreement with the D/H that was measured in the plume of water being released from the interior of Enceladus (41). Phoebe has an anomalously high D/H that is an exception compared to the other moons (42).

Comets provide the most detail about water isotopes. The variability of D/H among comets is discussed in the main article. The only cometary measurements of ¹⁶O/¹⁷O are for two species at 67P/C-G (32,61). Water is slightly enriched in the heavy isotope, both in previously published (32) results and in our work. Interestingly, O₂ is significantly enriched in ¹⁷O suggesting fractionating processes in the PSN (61). Measurements of ¹⁶O/¹⁸O in water are available for seven comets. All except C/2009 P1 Garradd have uncertainties that allow for terrestrial values. C/2009 P1 Garradd is depleted in the heavy isotope, ¹⁸O. Water in comet 67P/C-G is slightly enriched in the heavy isotope, similar to ¹⁶O/¹⁷O both in previously published analyses (36) and in our results. Measurements of ¹⁶O/¹⁸O in other species in the coma of 67P/C-G show significant variability, with terrestrial-like values in dust (62), CO₂ (63), and CH₃OH (61). Three sulfur-bearing species along with O₂ and H₂CO are all highly enriched in the heavy isotope (61), again showing signs of fractionation in the oxygen isotopes between species in the PSN.

Very few measurements are currently available for constraining the variability of D/H in methane in the PSN. Although the D/H ratio in methane in Titan's atmosphere is in the terrestrial range, the atmosphere has evolved over time and the primordial value was likely lower (64,65). The oxygen isotopes for Titan are slightly depleted in the heavy isotope relative to terrestrial values, but with error bars that allow for terrestrial isotope ratios (66). Recent measurements of D/H in methane on the surfaces of two Transneptunian Objects (TNOs), Eris and Makemake, show \sim 1.2–2.2 x enrichment over terrestrial values (67). However, atmospheric loss is likely to have enriched the isotopes allowing for the possibility of lower primordial values. The only D/H in cometary CH₄ was measured for 67P/C-G and was found to be enriched by more than 10x the terrestrial value (32). More measurements of D/H in cometary methane are needed to better understand how this species varied in the PSN.

Isotope and abundance trends over time

Figure 3 of the main article illustrates the visible variation of the isotope ratios and abundances with subspacecraft latitude and distance from the comet. We provide in Table S9 correlations for the time periods illustrated in this figure. The cells of the table are shaded based on whether the correlation is positive (purple) or negative (salmon) with a darker shade for stronger correlations. Cells with negligible correlations are not shaded.

In all four panels of Figure 3 the D/H ratio anti-correlates strongly with the ¹⁶O/¹⁷O meaning that the relative abundance of the heavier isotope compared to the lighter isotope increases or decreases together for both ratios. D/H correlates strongly with ¹⁶O/¹⁸O ratios during perihelion and post-perihelion but weakly or not at all pre-perihelion. The oxygen isotopes, ¹⁶O/¹⁷O and ¹⁶O/¹⁸O consistently correlate showing that their heavy isotopes vary together.

The hypervolatiles CO, CH₄, and HCN show weak to strong correlations with each other throughout the entire time evaluated. D/H weakly anticorrelates with the abundances of CO, CH₄, and HCN and ¹⁶O/¹⁷O weakly correlates with these species pre-perihelion during the earliest time of the mission (Figure 3A). The strongest anticorrelations are with CO and continue for D/H as the comet approaches perihelion (Figure 3B). This means that the heavy isotope is less abundant when these three species are more abundant pre-perihelion. ¹⁶O/¹⁸O anti-correlates with HCN and CO suggesting an opposite trend (Figures 3A & 3B). This is phase 3 of the dust cycle when “old” dust that is depleted in hypervolatiles like CO, CH₄, and HCN is re-released from the northern hemisphere.

During perihelion (Figure 3C) the correlation of the isotopes and these species is negligible. Although this is during phase 1 of the dust cycle, the spacecraft was at a distance greater than 120 km from the nucleus in a coma that was well-mixed. Post-perihelion (Figure 3D) the correlation with D/H is positive and is negative with the oxygen isotopes, meaning that the heavy isotope increases when the abundances of these species increase. This is during phase 2 of the dust cycle when the spacecraft was close to the comet and exposed to “new” dust being released from the nucleus. This dust is rapidly losing hypervolatiles prior to redeposition on the northern hemisphere.

During pre-perihelion (Figure 3A) D/H strongly correlates with latitude while ¹⁶O/¹⁷O strongly anticorrelates with latitude meaning that the heavy isotopes increase with increasing northern latitude. ¹⁶O/¹⁸O does not significantly correlate with latitude but has a weak positive correlation with distance such that the heavy isotope decreases with increasing distance from the nucleus. This is during phase 3 of the dust cycle where “old” dust is being released from the northern hemisphere.

The correlation between D/H and $^{16}\text{O}/^{17}\text{O}$ with distance is negligible early pre-perihelion (Figure 3A) but D/H develops a weak anticorrelation closer to perihelion (Figure 3B) such that the abundance of the heavy isotope decreases with increasing distance from the nucleus. $^{16}\text{O}/^{18}\text{O}$ correlations with distance and latitude during this same time (Figure 3B) show the opposite trends for the heavy isotope compared to D/H. The only correlation during perihelion (Figure 3C), when the spacecraft was at a distance where the coma was well-mixed, is a weak correlation between $^{16}\text{O}/^{17}\text{O}$ and latitude.

Post-perihelion (Figure 3D) D/H and $^{16}\text{O}/^{17}\text{O}$ weakly correlate with latitude where the heavy isotope decreases with increasing northern latitude. This is opposite to the correlation observed during the early pre-perihelion (Figure 3A) time period. D/H weakly anticorrelates with distance during this time. $^{16}\text{O}/^{18}\text{O}$ correlates with latitude opposite to the other two isotopes.

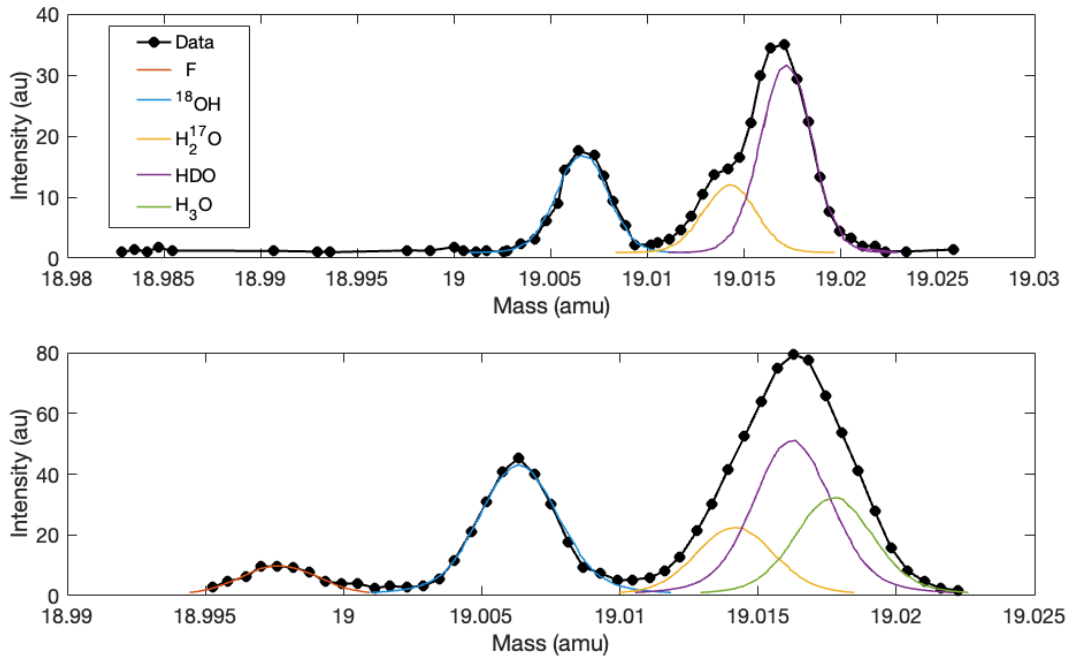


Fig. S1.

Illustration of published methods for fitting to mass 19. (top) Mass spectrum for mass 19 showing standard nonlinear least squares fits to F, ^{18}OH , HDO, and H_2^{17}O from Fig. 1 of (10) for 22 Aug. 2014. (bottom) Mass spectrum for mass 19 showing standard nonlinear least squares fits to F, ^{18}OH , HDO, H_2^{17}O , and H_3O from Fig. 1b of (32) for 07 May 2015.

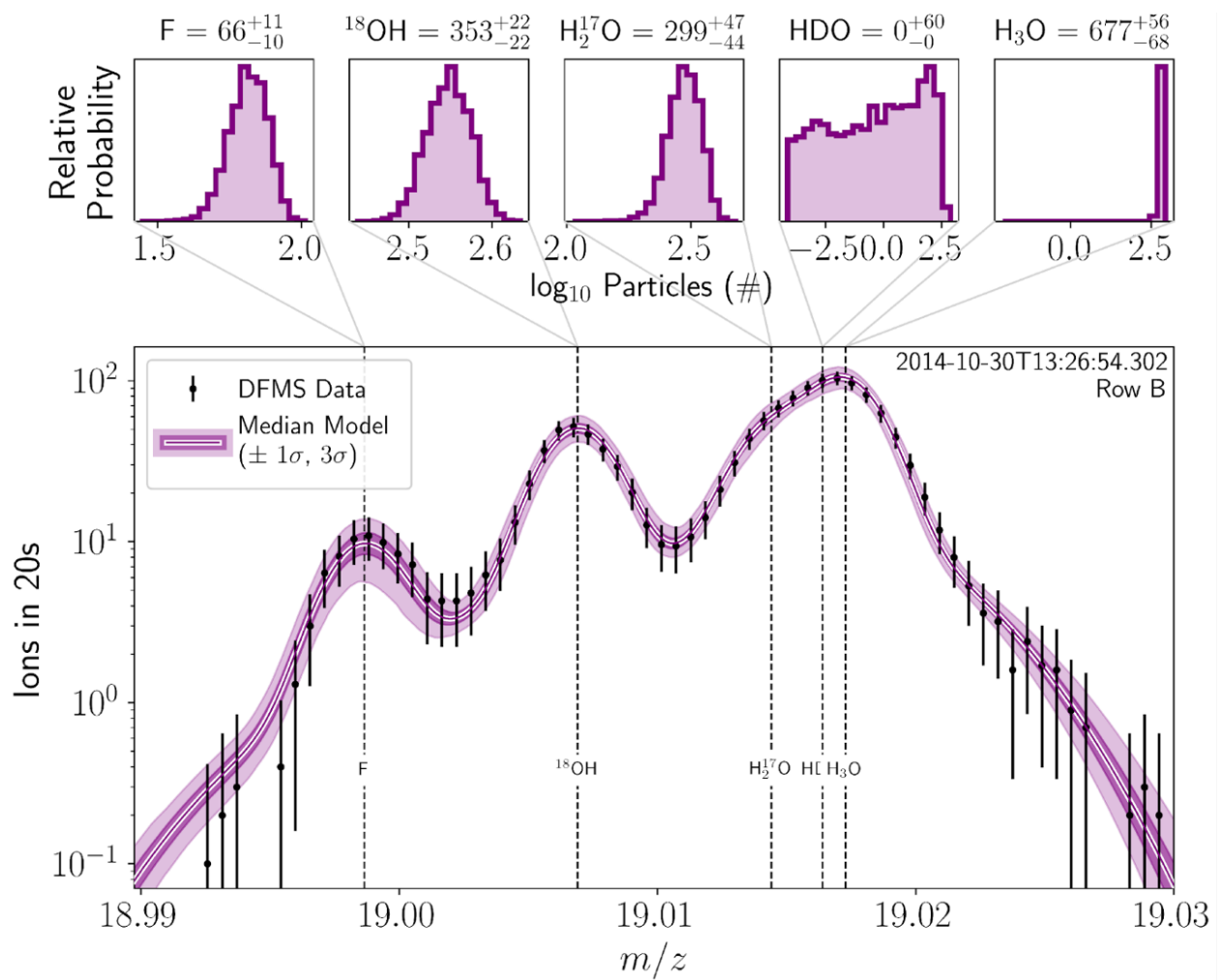


Fig. S2.

Probabilistic constraints on the number of each species (F, ^{18}OH , HDO, H_2^{17}O , and H_3O) inferred from Bayesian fits to mass 19 measurements. The upper row of panels shows the relative probability density of each species as histograms in units of \log_{10} the total number of particles. Each title indicates the median retrieved number of particles and 1-sigma credible intervals in linear space. The lower panel shows data from 30 October 2014 (black points with 1-sigma uncertainties) and our median fit to the spectrum (purple line with white outline). The median fit is bounded by 1-sigma and 3-sigma credibility envelopes (dark and light purple shading, respectively) that depict the range of model fits to the spectrum that are consistent with the particle numbers constraints shown in the upper panels.

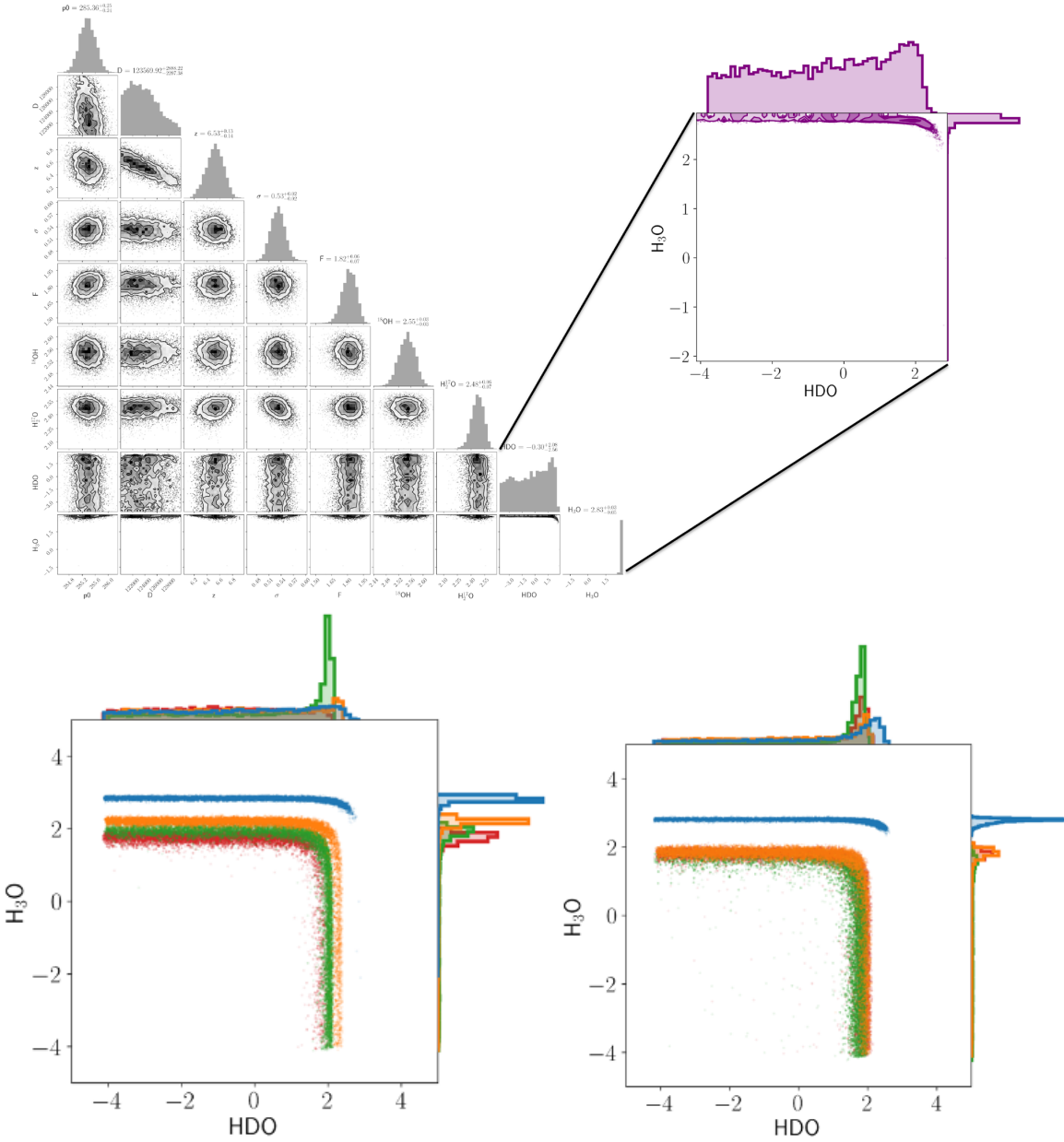


Fig. S3.

Since the peaks of HDO and H_3O significantly overlap on the detector, a strong degeneracy is seen between the two species, making them difficult to uniquely identify. The upper left matrix of subpanels shows 1D and 2D marginalized posterior distributions for each model fitting parameter for a fit to a single DFMS measurement. The right panel zooms into the covariance between HDO and H_3O . This shows that the H_3O peak can remain large over orders of magnitude in the signal from HDO, until HDO becomes equally large and the two species switch roles with HDO high and H_3O low. The lower panels (Row A on left, Row B on right) demonstrate this same effect for four separate measurement fits, where the same “right angle” bend in the HDO- H_3O covariance is seen along the line of $\text{HDO}=\text{H}_3\text{O}$ ($x=y$), albeit offset to account for the different peak heights of each measurement.

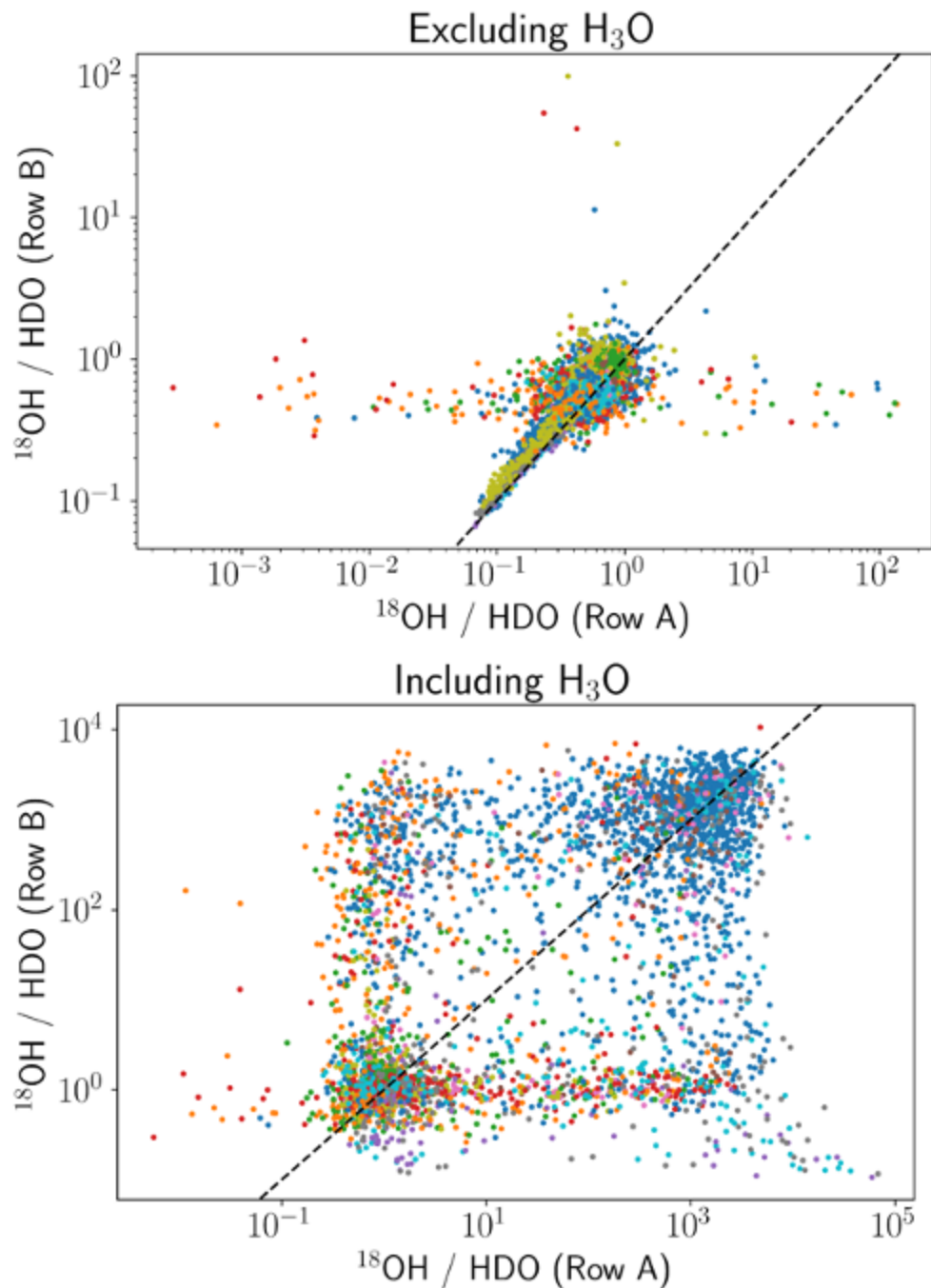


Fig. S4.

The ratio of the derived signals for all of the fits to Mass 19, including the fits where the signal to noise is poor. In a fit with good signal to noise, ^{18}OH to HDO should be the same on both detector rows. This is generally the case when the fit is done without H_3O (top panel) but is not the case when H_3O is included in the fit (bottom panel). Note that the outliers in the top panel are the result of spillover in the detector and are excluded from further analysis.

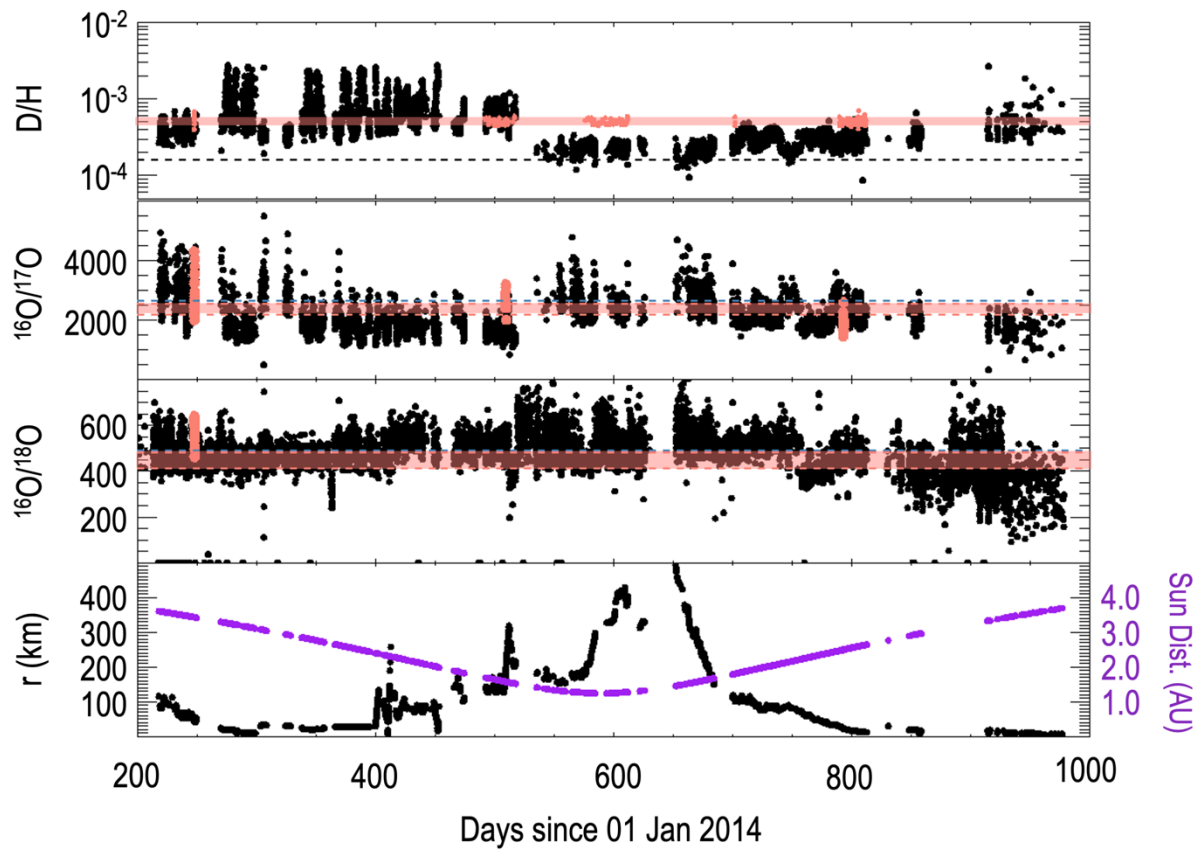


Fig. S5.

Observations of the isotope ratios in water over the full mission dataset. The values derived here are shown in black and compared to published values for D/H (10,32,34), $^{16}\text{O}/^{17}\text{O}$ (32), and $^{16}\text{O}/^{18}\text{O}$ (36) shown in salmon. The bottom panel shows the distance of the spacecraft from the comet nucleus in km (black) and the distance of the comet and spacecraft from the Sun (purple).

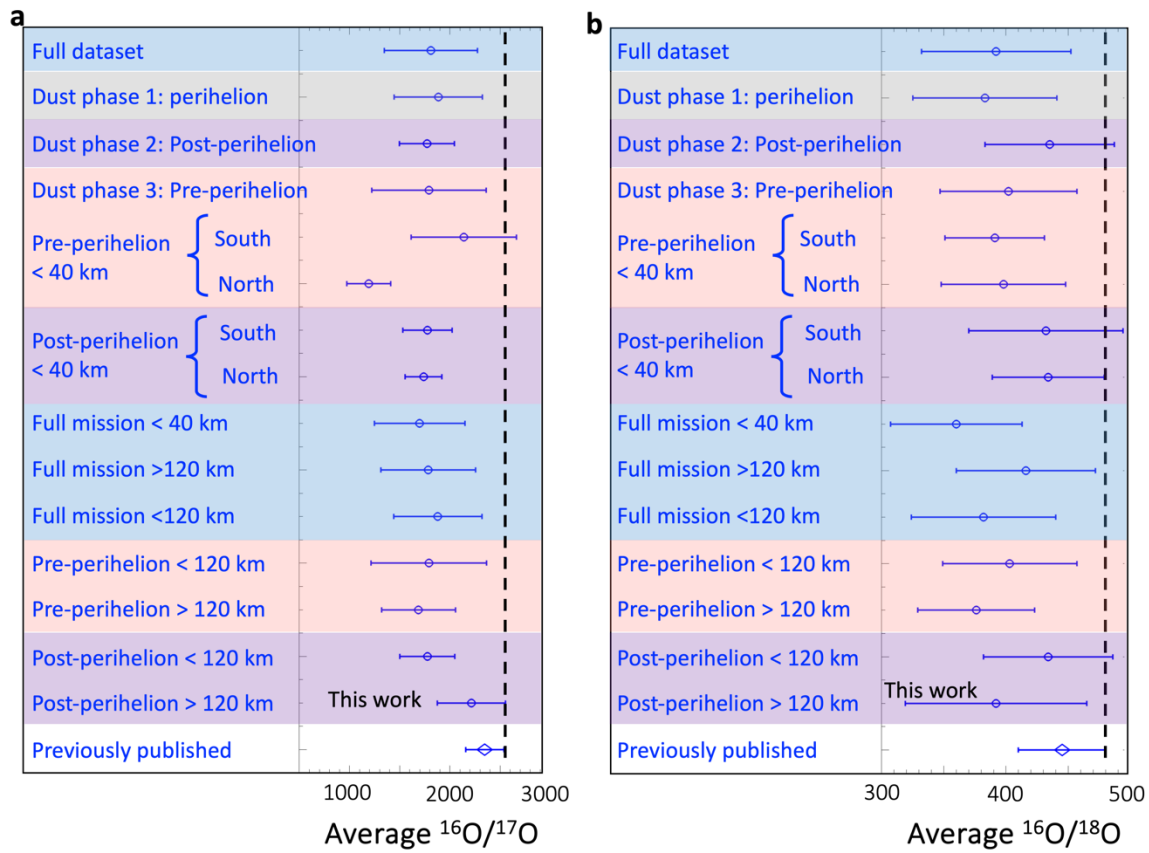


Figure S6.

Average and standard deviation for the oxygen isotopes in water measured during different time periods of the mission. Colors represent the phases of the dust cycle described earlier. Phase 1 is perihelion (gray), phase 2 is postperihelion (purple), and phase 3 is pre-perihelion (salmon). Error bars indicate how much the isotope ratio varies within each group (See Fig. 4 of main article for D/H). The dashed line corresponds to the Vienna Standard Mean Ocean Water (VSMOW) value.

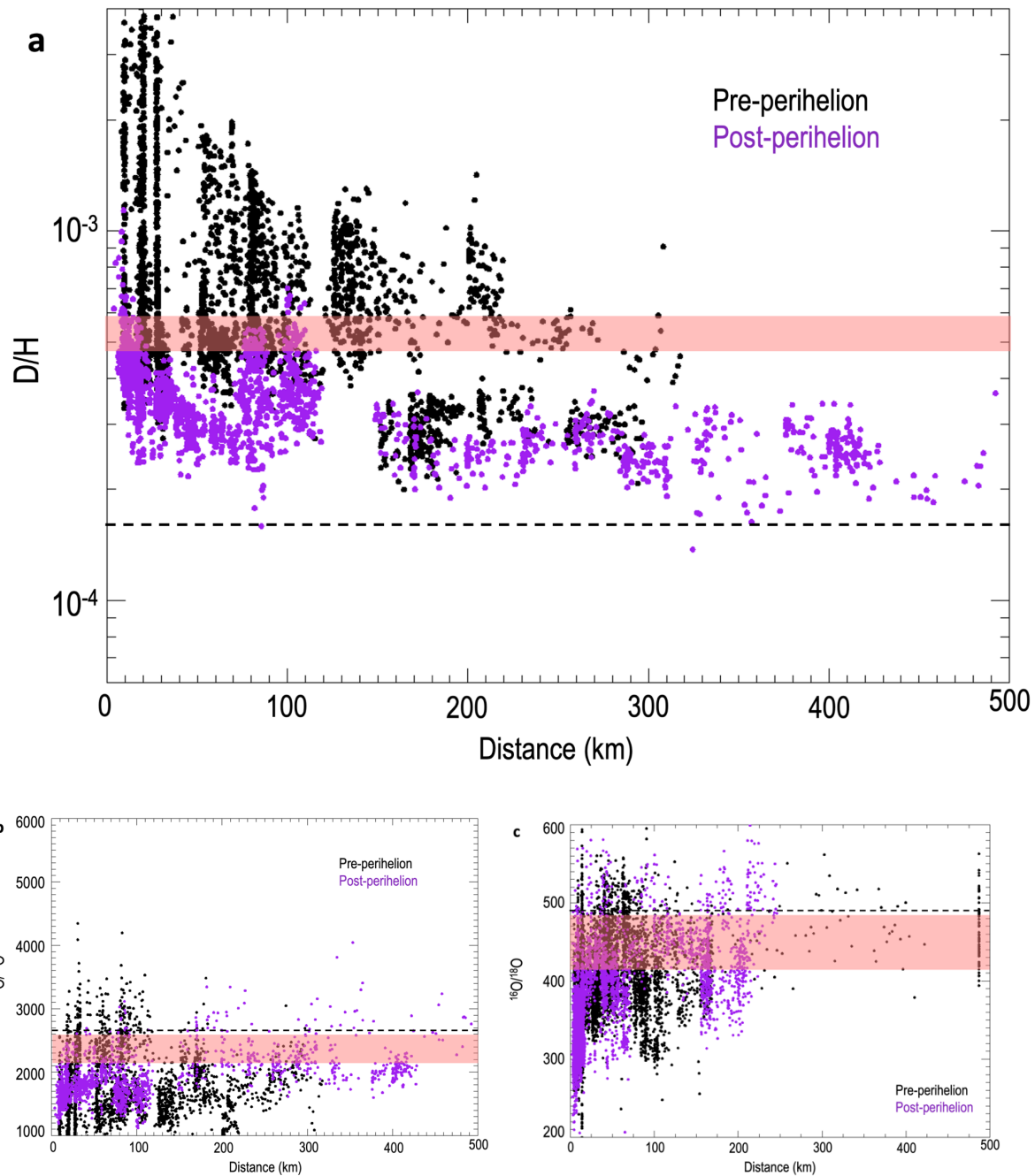


Fig. S7.

All individual measurements of the water isotopes as a function of distance for pre-perihelion (black) and post-perihelion (purple). The published value ranges are shown by the salmon shaded region.

Table S1.

Measurements of D/H throughout the solar system illustrated in Figure 1.

		Isotope ratio	Molecule	Reference
Sun		(2.1±0.5) x 10 ⁻⁵	H	(68)
PSN		(2.6±0.7) x 10 ⁻⁵	H	(3)
Jupiter		(2.6±0.7) x 10 ⁻⁵	H ₂	(3)
Saturn		(1.7±0.7) x 10 ⁻⁵	H ₂	(54)
Uranus		(4.4±0.4) x 10 ⁻⁵	H ₂	(56)
Neptune		(4.1±0.4) x 10 ⁻⁵	H ₂	(56)
Venus		(1.6±0.2) x 10 ⁻²	H ₂ O	(69)
Mars		(8.6±4.0) x 10 ⁻⁴	H ₂ O	(70)
Chondrites	CI	(1.68±0.11) x 10 ⁻⁴	Hydrates	(58)
	CM	(1.47±0.21) x 10 ⁻⁴		
	CV	(1.58±0.16) x 10 ⁻⁴		
	CO	(1.48±0.15) x 10 ⁻⁴		
	CR	(2.26±0.22) x 10 ⁻⁴		
	LL	(4.08±0.40) x 10 ⁻⁴		
	EH	(1.54±0.05) x 10 ⁻⁴		
	EL	(1.38±0.01) x 10 ⁻⁴		
Saturn's moons	Enceladus	(2.9±1.5) x 10 ⁻⁴	H ₂ O	(41)
	Hyperion	(2.15±0.75) x 10 ⁻⁴	H ₂ O	(42)
	Rhea	(1.8±0.3) x 10 ⁻⁴	H ₂ O	
	Iapetus	(1.7±0.3) x 10 ⁻⁴	H ₂ O	
	Phoebe	(1.3±0.3) x 10 ⁻³	H ₂ O	
	Titan	(1.59±0.33) x 10 ⁻⁴	CH ₄	(71)
Eris		(2.5±0.5) x 10 ⁻⁴	CH ₄	(67)
Makemake		(2.9±0.6) x 10 ⁻⁴	CH ₄	
OCCs	1P/Halley	(3.08±0.5) x 10 ⁻⁴	H ₂ O	(72)
		(3.06±0.34) x 10 ⁻⁴	H ₂ O	(73)
		(2.1±0.3) x 10 ⁻⁴	H ₂ O	(25)
	C/1996 B2	(2.9±1.0) x 10 ⁻⁴	H ₂ O	(74)
		(1.85±0.6) x 10 ⁻⁴	H ₂ O	(12)
	C/1995 O1	(3.3±0.8) x 10 ⁻⁴	H ₂ O	(75)
	8P/Tuttle	(4.09±1.45) x 10 ⁻⁴	H ₂ O	(76)
	C/2009 P1	(2.06±0.22) x 10 ⁻⁴	H ₂ O	(77)

		Isotope ratio	Molecule	Reference
OCCs (cont.)	153P/I-Z	$< 2.5 \times 10^{-4}$	H ₂ O	(13)
	C/2007 N3	$< 5.6 \times 10^{-4}$	H ₂ O	(14)
	C/2002 T7	$(2.5 \pm 0.7) \times 10^{-4}$	H ₂ O	(78)
	C/2001 Q4	$(4.6 \pm 1.4) \times 10^{-4}$	H ₂ O	(79)
	C/2012 F6	$(6.5 \pm 1.6) \times 10^{-4}$	H ₂ O	(15)
	C/2014 Q2	$(1.4 \pm 0.4) \times 10^{-4}$	H ₂ O	(15)
		$(3.02 \pm 0.87) \times 10^{-4}$	H ₂ O	(16)
JFCs	45P/H-M-P	$< 2 \times 10^{-4}$	H ₂ O	(11)
	103P/H2	$(1.61 \pm 0.24) \times 10^{-4}$	H ₂ O	(6)
	46P/Wirt.	$(1.61 \pm 0.65) \times 10^{-4}$	H ₂ O	(12)
	67P/C-G	$(5.01 \pm 0.41) \times 10^{-4}$	H ₂ O	(32)
		$(2.41 \pm 0.29) \times 10^{-3}$	CH ₄	(32)
		$(1.57 \pm 0.54) \times 10^{-3}$	Organics	(62)
		$(2.59 \pm 0.36) \times 10^{-4}$	H₂O	This work
VSMOW	Earth	1.56×10^{-4}	H₂O	

Table S2.Measurements of $^{16}\text{O}/^{17}\text{O}$ throughout the solar system.

		Isotope ratio	Molecule	Reference
Sun		2696±642	O	(53)
Mars		2655±25	H ₂ O	(70)
Chondrites	CI	2623.9	H ₂ O	(59, 60)
	CM	2631.6		
	CV	2633.7		
	CO	2636.7		
	CR	2627.5		
Saturn's moons	Titan	2917±359	CO	(66)
JFCs	67P/C-G	2347±191	H ₂ O	(29)
		1544±308	O ₂	(61)
		2214±340	H₂O	This work
VSMOW	Earth	2625	H ₂ O	

Table S3.Measurements of $^{16}\text{O}/^{18}\text{O}$ throughout the solar system.

		Isotope ratio	Molecule	Reference
Sun		499±119	O	(53)
Jupiter		243±203	H ₂ O	(57)
Venus		500±26	H ₂ O	(80)
Mars		490±25	H ₂ O	(70)
Chondrites	CI	497.5±0.2	H ₂ O	(59,60)
	CM	481.24±0.93		
	CV	485.6		
	CO	483.3±5.0		
	CR	482.4±1.0		
	EH	481.3±1.0		
	EL	478.5±2.0		
Saturn's moons	Titan	486±22	CO	(66)
OCCs	1P/Halley	518±45	H ₂ O	(72)
		470±40	H ₂ O	(73)
	C/2009 P1	523±32	H ₂ O	(77)
	C/2002 T7	425±55	H ₂ O	(78)
	C/2014	499±24	H ₂ O	(15)
JFCs	103P/H2	500±50	H ₂ O	(6)
	67P/C-G	494±8	CO ₂	(63)
		495±40	CH ₃ OH	(61)
		345±40	O ₂	(61)
		256±100	H ₂ CO	(61)
		239±52	SO	(61)
		248±88	SO ₂	(61)
		277±70	OCS	(61)
		495±40	Dust	(62)
		445±35	H ₂ O	(36)
		392±73	H₂O	This work
VSMOW	Earth	486.6	H ₂ O	

Table S4.

Parameters and their respective prior probability distributions for fits to the mass 19 DFMS data. $\text{Normal}(\text{mean}, \text{std})$ denotes a Gaussian probability distribution in terms of the mean and standard deviation and $\text{Uniform}(\text{lower}, \text{upper})$ denotes a flat uniform probability distribution in terms of lower and upper bounds. The p_0 mean and standard deviation are set based on the values in the data header.

Parameter	Description	Prior Probability Distribution
p_0	Pixel where the commanded mass m_0 is located	$\text{Normal}(\text{ROSINA_DFMS_SCI_SELF_PIXEL0_A}, \text{ROSINA_DFMS_SCI_SELF_PIXEL0_UNCA})$
D	Dispersion factor	$\text{Uniform}(120000, 130000)$
z	Zoom factor	$\text{Normal}(6.6, 0.2)$
$\log_{10}(c)$	Width of first Gaussian	$\text{Uniform}(0,2)$
$\log_{10}(a_i)$	Logarithm of the amplitude of first Gaussian for the i -th species, used for F, ^{18}OH , H_2^{17}O , HDO, and H_3O^+	$\text{Uniform}(-5, 5)$

Table S5.

Comparison of measurements reported in (10, 32, and 34) with the results from this work. The quality note indicates which measurements were excluded from our analysis due to the large uncertainty in the fit to mass 19 using NS methods described above.

Date and time of measurement	Published	Error	This work	Error	Ref.	Quality note
2014-09-04T18:14:25.920	5.69×10^{-4}	1.14×10^{-4}	5.68×10^{-4}	4.44×10^{-5}	(10)	Excluded
2014-09-04T18:35:42.807	3.97×10^{-4}	7.93×10^{-5}	5.27×10^{-4}	4.30×10^{-5}	(10)	Excluded
2014-09-04T18:57:01.864	5.52×10^{-4}	1.10×10^{-4}	6.04×10^{-4}	4.86×10^{-5}	(10)	Excluded
2014-09-04T19:18:22.708	6.27×10^{-4}	1.25×10^{-4}	6.05×10^{-4}	4.72×10^{-5}	(10)	Excluded
2014-09-04T19:39:45.714	5.65×10^{-4}	1.13×10^{-4}	6.50×10^{-4}	5.08×10^{-5}	(10)	Excluded
2014-09-04T20:00:56.793	6.71×10^{-4}	1.34×10^{-4}	5.97×10^{-4}	4.67×10^{-5}	(10)	Excluded
2014-09-04T20:22:21.880	5.48×10^{-4}	1.10×10^{-4}	5.40×10^{-4}	4.22×10^{-5}	(10)	
2014-09-04T20:43:32.997	6.76×10^{-4}	1.35×10^{-4}	5.77×10^{-4}	4.50×10^{-5}	(10)	
2014-09-04T21:05:03.852	5.69×10^{-4}	1.14×10^{-4}	5.31×10^{-4}	4.15×10^{-5}	(10)	
2014-09-04T21:26:16.920	5.86×10^{-4}	1.17×10^{-4}	5.37×10^{-4}	4.19×10^{-5}	(10)	
2014-09-04T23:22:33.968	5.32×10^{-4}	1.06×10^{-4}	4.72×10^{-4}	3.70×10^{-5}	(10)	
2014-09-04T23:52:41.046	5.36×10^{-4}	1.07×10^{-4}	4.63×10^{-4}	3.62×10^{-5}	(10)	
2014-09-05T00:14:05.953	4.64×10^{-4}	9.29×10^{-5}	4.92×10^{-4}	3.88×10^{-5}	(10)	
2014-09-05T00:35:24.784	5.44×10^{-4}	1.09×10^{-4}	4.74×10^{-4}	3.70×10^{-5}	(10)	
2014-09-05T01:18:00.448	5.40×10^{-4}	1.08×10^{-4}	7.12×10^{-4}	5.56×10^{-5}	(10)	Excluded
2014-09-05T01:39:17.328	5.20×10^{-4}	1.04×10^{-4}	5.65×10^{-4}	4.41×10^{-5}	(10)	
2014-09-05T02:00:36.124	5.86×10^{-4}	1.17×10^{-4}	6.20×10^{-4}	4.84×10^{-5}	(10)	Excluded
2014-09-05T02:21:54.966	5.28×10^{-4}	1.06×10^{-4}	6.21×10^{-4}	4.85×10^{-5}	(10)	
2014-09-05T02:43:09.883	5.44×10^{-4}	1.09×10^{-4}	5.73×10^{-4}	4.47×10^{-5}	(10)	
2014-09-05T03:04:34.712	5.65×10^{-4}	1.13×10^{-4}	6.10×10^{-4}	4.77×10^{-5}	(10)	
2014-09-05T03:25:57.479	5.52×10^{-4}	1.10×10^{-4}	6.85×10^{-4}	5.35×10^{-5}	(10)	Excluded
2014-09-05T03:47:20.399	5.86×10^{-4}	1.17×10^{-4}	6.43×10^{-4}	5.03×10^{-5}	(10)	Excluded
2014-09-05T04:08:39.244	5.32×10^{-4}	1.06×10^{-4}	5.31×10^{-4}	4.15×10^{-5}	(10)	Excluded
2014-09-05T04:30:06.171	5.40×10^{-4}	1.08×10^{-4}	5.22×10^{-4}	4.08×10^{-5}	(10)	Excluded
2014-09-05T04:51:22.951	5.60×10^{-4}	1.12×10^{-4}	4.83×10^{-4}	3.77×10^{-5}	(10)	Excluded
2014-09-05T05:12:33.868	5.56×10^{-4}	1.11×10^{-4}	4.91×10^{-4}	3.86×10^{-5}	(10)	Excluded
2015-05-06T12:27:40.900	5.54×10^{-4}	1.11×10^{-4}	6.51×10^{-4}	5.09×10^{-5}	(32)	Excluded
2015-05-07T22:56:23.692	5.58×10^{-4}	1.12×10^{-4}	5.07×10^{-4}	3.96×10^{-5}	(32)	
2015-05-08T01:26:21.876	5.26×10^{-4}	1.05×10^{-4}	4.39×10^{-4}	3.43×10^{-5}	(32)	
2015-05-10T02:00:00.653	4.58×10^{-4}	9.16×10^{-5}	5.09×10^{-4}	3.98×10^{-5}	(32)	
2015-05-10T10:35:13.035	4.97×10^{-4}	9.94×10^{-5}	9.99×10^{-4}	7.80×10^{-5}	(32)	
2015-05-10T14:53:59.713	5.16×10^{-4}	1.03×10^{-4}	5.03×10^{-4}	3.93×10^{-5}	(32)	

Date and time of measurement	Published	Error	This work	Error	Ref.	Quality note
2015-05-10T21:00:15.851	5.56×10^{-4}	1.11×10^{-4}	5.63×10^{-4}	4.40×10^{-5}	(32)	
2015-05-11T01:16:50.110	4.99×10^{-4}	9.98×10^{-5}	9.08×10^{-4}	7.09×10^{-5}	(32)	
2015-05-11T05:17:58.250	5.40×10^{-4}	1.08×10^{-4}	6.99×10^{-4}	5.46×10^{-5}	(32)	Excluded
2015-05-14T22:53:37.044	5.33×10^{-4}	1.07×10^{-4}	9.53×10^{-4}	7.44×10^{-5}	(32)	
2015-05-14T19:56:36.763	4.90×10^{-4}	9.79×10^{-5}	6.71×10^{-4}	5.24×10^{-5}	(32)	Excluded
2015-05-15T01:09:37.764	4.46×10^{-4}	8.92×10^{-5}	4.39×10^{-4}	3.43×10^{-5}	(32)	Excluded
2015-05-15T11:51:38.813	4.87×10^{-4}	9.75×10^{-5}	9.99×10^{-4}	7.80×10^{-5}	(32)	
2015-05-15T22:06:40.996	5.11×10^{-4}	1.02×10^{-4}	8.91×10^{-4}	6.96×10^{-5}	(32)	
2015-05-16T16:38:23.629	5.09×10^{-4}	1.02×10^{-4}	5.90×10^{-4}	4.61×10^{-5}	(32)	
2015-05-17T04:50:28.137	4.96×10^{-4}	9.92×10^{-5}	7.08×10^{-4}	5.53×10^{-5}	(32)	Excluded
2015-05-17T12:45:46.434	4.57×10^{-4}	9.13×10^{-5}	8.76×10^{-4}	6.84×10^{-5}	(32)	
2015-05-18T04:32:39.210	5.19×10^{-4}	1.04×10^{-4}	8.35×10^{-4}	6.52×10^{-5}	(32)	
2015-05-18T09:33:33.114	4.46×10^{-4}	8.91×10^{-5}	8.75×10^{-4}	6.83×10^{-5}	(32)	
2015-05-18T19:36:40.706	4.76×10^{-4}	9.52×10^{-5}	6.54×10^{-4}	5.11×10^{-5}	(32)	
2015-05-19T06:23:46.410	5.61×10^{-4}	1.12×10^{-4}	5.43×10^{-4}	4.24×10^{-5}	(32)	
2015-05-19T06:23:46.410	5.04×10^{-4}	1.01×10^{-4}	5.43×10^{-4}	4.24×10^{-5}	(32)	
2015-05-21T02:18:36.049	4.86×10^{-4}	9.73×10^{-5}	7.33×10^{-4}	5.73×10^{-5}	(32)	Excluded
2015-05-21T14:41:54.668	4.52×10^{-4}	9.03×10^{-5}	7.70×10^{-4}	6.01×10^{-5}	(32)	Excluded
2015-05-23T16:22:31.801	4.90×10^{-4}	9.81×10^{-5}	7.88×10^{-4}	6.15×10^{-5}	(32)	Excluded
2015-05-23T23:59:31.717	5.16×10^{-4}	1.03×10^{-4}	6.42×10^{-4}	5.01×10^{-5}	(32)	
2015-05-23T23:59:31.717	4.49×10^{-4}	8.98×10^{-5}	6.42×10^{-4}	5.01×10^{-5}	(32)	
2015-05-24T04:17:42.597	4.68×10^{-4}	9.37×10^{-5}	6.46×10^{-4}	5.04×10^{-5}	(32)	
2015-05-24T13:21:54.892	5.38×10^{-4}	1.08×10^{-4}	8.13×10^{-4}	6.35×10^{-5}	(32)	
2015-05-25T07:28:07.326	5.42×10^{-4}	1.08×10^{-4}	5.52×10^{-4}	4.31×10^{-5}	(32)	
2015-05-25T09:37:00.196	5.23×10^{-4}	1.05×10^{-4}	5.59×10^{-4}	4.37×10^{-5}	(32)	
2015-05-25T06:45:11.963	4.88×10^{-4}	9.76×10^{-5}	5.71×10^{-4}	4.46×10^{-5}	(32)	
2015-05-26T04:27:06.666	5.29×10^{-4}	1.06×10^{-4}	5.52×10^{-4}	4.31×10^{-5}	(32)	Excluded
2015-05-26T01:34:56.778	5.16×10^{-4}	1.03×10^{-4}	4.94×10^{-4}	3.86×10^{-5}	(32)	
2015-05-26T00:51:53.351	4.83×10^{-4}	9.67×10^{-5}	4.89×10^{-4}	3.82×10^{-5}	(32)	Excluded
2015-05-26T08:28:31.910	4.59×10^{-4}	9.19×10^{-5}	5.38×10^{-4}	4.20×10^{-5}	(32)	
2015-05-26T21:55:06.909	5.03×10^{-4}	1.01×10^{-4}	4.53×10^{-4}	3.57×10^{-5}	(32)	
2015-05-31T00:33:29.389	4.98×10^{-4}	9.95×10^{-5}	7.10×10^{-4}	5.55×10^{-5}	(32)	
2015-05-31T23:32:41.122	5.61×10^{-4}	1.12×10^{-4}	8.89×10^{-4}	6.95×10^{-5}	(32)	
2015-06-01T00:16:01.182	5.95×10^{-4}	1.19×10^{-4}	9.47×10^{-4}	7.40×10^{-5}	(32)	
2015-07-30T11:47:17.979	5.22×10^{-4}	1.04×10^{-4}	5.48×10^{-4}	4.28×10^{-5}	(32)	Excluded
2015-07-30T18:26:18.990	5.22×10^{-4}	1.04×10^{-4}	3.19×10^{-4}	2.49×10^{-5}	(32)	
2015-07-31T15:35:23.375	5.28×10^{-4}	1.06×10^{-4}	3.33×10^{-4}	2.60×10^{-5}	(32)	Excluded

Date and time of measurement	Published	Error	This work	Error	Ref.	Quality note
2015-08-01T20:48:26.221	5.63×10^{-4}	1.13×10^{-4}	2.91×10^{-4}	2.27×10^{-5}	(32)	
2015-08-02T09:53:16.112	5.37×10^{-4}	1.07×10^{-4}	3.50×10^{-4}	2.73×10^{-5}	(32)	
2015-08-04T11:25:20.637	5.59×10^{-4}	1.12×10^{-4}	3.52×10^{-4}	2.75×10^{-5}	(32)	
2015-08-05T10:54:16.634	5.02×10^{-4}	1.00×10^{-4}	2.89×10^{-4}	2.25×10^{-5}	(32)	
2015-08-05T15:21:18.907	4.96×10^{-4}	9.91×10^{-5}	2.70×10^{-4}	2.11×10^{-5}	(32)	
2015-08-05T18:56:19.426	4.52×10^{-4}	9.04×10^{-5}	3.24×10^{-4}	2.53×10^{-5}	(32)	
2015-08-06T15:22:18.612	4.61×10^{-4}	9.22×10^{-5}	2.81×10^{-4}	2.20×10^{-5}	(32)	
2015-08-06T12:30:18.412	5.33×10^{-4}	1.07×10^{-4}	2.93×10^{-4}	2.29×10^{-5}	(32)	
2015-08-06T19:08:17.060	4.85×10^{-4}	9.70×10^{-5}	3.13×10^{-4}	2.45×10^{-5}	(32)	
2015-08-07T13:59:21.973	4.91×10^{-4}	9.83×10^{-5}	3.32×10^{-4}	2.59×10^{-5}	(32)	
2015-08-09T16:54:20.667	4.57×10^{-4}	9.13×10^{-5}	5.64×10^{-4}	4.41×10^{-5}	(32)	Excluded
2015-08-10T10:59:05.748	4.48×10^{-4}	8.96×10^{-5}	3.56×10^{-4}	2.78×10^{-5}	(32)	Excluded
2015-08-10T18:10:16.196	4.83×10^{-4}	9.65×10^{-5}	4.26×10^{-4}	3.33×10^{-5}	(32)	Excluded
2015-08-13T09:38:51.836	4.76×10^{-4}	9.52×10^{-5}	4.49×10^{-4}	3.51×10^{-5}	(32)	Excluded
2015-08-13T09:38:51.836	5.04×10^{-4}	1.01×10^{-4}	4.49×10^{-4}	3.51×10^{-5}	(32)	Excluded
2015-08-14T00:09:46.027	5.33×10^{-4}	1.07×10^{-4}	4.19×10^{-4}	3.28×10^{-5}	(32)	Excluded
2015-08-15T07:42:30.018	4.78×10^{-4}	9.57×10^{-5}	3.96×10^{-4}	3.09×10^{-5}	(32)	Excluded
2015-08-16T04:51:35.541	5.57×10^{-4}	1.11×10^{-4}	4.71×10^{-4}	3.68×10^{-5}	(32)	Excluded
2015-08-17T00:58:49.033	4.57×10^{-4}	9.13×10^{-5}	2.75×10^{-4}	2.15×10^{-5}	(32)	Excluded
2015-08-17T23:04:26.419	4.72×10^{-4}	9.43×10^{-5}	4.16×10^{-4}	3.25×10^{-5}	(32)	Excluded
2015-08-19T10:55:16.405	4.54×10^{-4}	9.09×10^{-5}	2.06×10^{-4}	1.61×10^{-5}	(32)	Excluded
2015-08-20T07:20:55.890	4.74×10^{-4}	9.48×10^{-5}	2.38×10^{-4}	1.86×10^{-5}	(32)	
2015-08-20T10:21:58.079	5.46×10^{-4}	1.09×10^{-4}	5.32×10^{-4}	4.15×10^{-5}	(32)	Excluded
2015-08-20T21:17:40.801	5.54×10^{-4}	1.11×10^{-4}	3.70×10^{-4}	2.89×10^{-5}	(32)	Excluded
2015-08-21T00:52:53.473	4.96×10^{-4}	9.91×10^{-5}	4.71×10^{-4}	3.68×10^{-5}	(32)	Excluded
2015-08-22T11:37:27.460	4.83×10^{-4}	9.65×10^{-5}	3.18×10^{-4}	2.48×10^{-5}	(32)	Excluded
2015-08-22T18:47:27.835	4.63×10^{-4}	9.26×10^{-5}	3.09×10^{-4}	2.41×10^{-5}	(32)	
2015-08-23T12:45:15.888	5.15×10^{-4}	1.03×10^{-4}	3.34×10^{-4}	2.61×10^{-5}	(32)	
2015-08-23T19:56:25.361	5.09×10^{-4}	1.02×10^{-4}	2.92×10^{-4}	2.29×10^{-5}	(32)	
2015-08-25T07:06:53.153	5.20×10^{-4}	1.04×10^{-4}	2.97×10^{-4}	2.32×10^{-5}	(32)	
2015-08-25T13:34:32.784	4.96×10^{-4}	9.91×10^{-5}	3.12×10^{-4}	2.44×10^{-5}	(32)	Excluded
2015-08-24T19:37:54.815	4.65×10^{-4}	9.30×10^{-5}	4.27×10^{-4}	3.34×10^{-5}	(32)	Excluded
2015-08-28T03:46:45.025	4.91×10^{-4}	9.83×10^{-5}	2.52×10^{-4}	1.97×10^{-5}	(32)	Excluded
2015-08-28T08:46:35.291	5.43×10^{-4}	1.09×10^{-4}	2.73×10^{-4}	2.14×10^{-5}	(32)	
2015-08-28T12:21:31.492	5.11×10^{-4}	1.02×10^{-4}	2.38×10^{-4}	1.86×10^{-5}	(32)	
2015-08-28T18:59:35.878	4.98×10^{-4}	9.96×10^{-5}	1.94×10^{-4}	1.51×10^{-5}	(32)	Excluded
2015-08-30T02:34:04.848	4.52×10^{-4}	9.04×10^{-5}	2.53×10^{-4}	1.98×10^{-5}	(32)	Excluded

Date and time of measurement	Published	Error	This work	Error	Ref.	Quality note
2015-08-30T09:42:47.213	4.93×10^{-4}	9.87×10^{-5}	2.33×10^{-4}	1.82×10^{-5}	(32)	
2015-08-29T20:50:47.369	4.65×10^{-4}	9.30×10^{-5}	4.37×10^{-4}	3.42×10^{-5}	(32)	Excluded
2015-08-30T13:17:59.456	4.74×10^{-4}	9.48×10^{-5}	2.65×10^{-4}	2.07×10^{-5}	(32)	
2015-08-31T00:05:10.087	4.61×10^{-4}	9.22×10^{-5}	2.40×10^{-4}	1.87×10^{-5}	(32)	
2015-08-30T16:55:59.612	5.28×10^{-4}	1.06×10^{-4}	2.46×10^{-4}	1.93×10^{-5}	(32)	
2015-08-30T20:29:59.837	5.13×10^{-4}	1.03×10^{-4}	2.47×10^{-4}	1.93×10^{-5}	(32)	
2015-09-02T11:47:15.669	4.59×10^{-4}	9.17×10^{-5}	2.64×10^{-4}	2.06×10^{-5}	(32)	
2015-09-02T15:22:07.871	4.78×10^{-4}	9.57×10^{-5}	2.45×10^{-4}	1.91×10^{-5}	(32)	
2015-09-03T01:36:35.634	4.87×10^{-4}	9.74×10^{-5}	2.85×10^{-4}	2.23×10^{-5}	(32)	
2015-09-02T22:43:57.452	5.00×10^{-4}	1.00×10^{-4}	2.90×10^{-4}	2.26×10^{-5}	(32)	Excluded
2015-09-03T15:23:00.356	5.20×10^{-4}	1.04×10^{-4}	3.08×10^{-4}	2.40×10^{-5}	(32)	
2015-09-04T06:04:42.583	5.43×10^{-4}	1.09×10^{-4}	2.30×10^{-4}	1.79×10^{-5}	(32)	
2015-09-03T22:44:42.236	5.85×10^{-4}	1.17×10^{-4}	5.26×10^{-4}	4.11×10^{-5}	(32)	Excluded
2015-12-03T07:20:36.195	5.74×10^{-4}	1.15×10^{-4}	3.59×10^{-4}	2.80×10^{-5}	(32)	
2015-12-03T08:53:53.915	5.77×10^{-4}	1.15×10^{-4}	3.83×10^{-4}	3.00×10^{-5}	(34)	
2015-12-03T10:18:38.662	4.42×10^{-4}	8.84×10^{-5}	6.04×10^{-4}	4.72×10^{-5}	(34)	Excluded
2015-12-03T12:46:33.742	4.89×10^{-4}	9.78×10^{-5}	3.78×10^{-4}	2.96×10^{-5}	(34)	
2016-02-28T02:43:07.643	5.77×10^{-4}	1.15×10^{-4}	4.30×10^{-4}	3.40×10^{-5}	(32)	Excluded
2016-02-28T04:09:16.641	4.42×10^{-4}	8.84×10^{-5}	6.12×10^{-4}	4.78×10^{-5}	(32)	Excluded
2016-02-28T16:55:04.316	4.85×10^{-4}	9.71×10^{-5}	3.57×10^{-4}	2.79×10^{-5}	(32)	
2016-02-28T21:22:51.946	4.85×10^{-4}	9.71×10^{-5}	5.86×10^{-4}	4.58×10^{-5}	(32)	Excluded
2016-03-01T01:22:56.265	5.47×10^{-4}	1.09×10^{-4}	3.48×10^{-4}	2.71×10^{-5}	(32)	
2016-03-01T21:28:56.332	4.98×10^{-4}	9.97×10^{-5}	3.46×10^{-4}	2.70×10^{-5}	(32)	
2016-03-01T22:12:19.827	4.39×10^{-4}	8.79×10^{-5}	4.08×10^{-4}	3.18×10^{-5}	(32)	Excluded
2016-03-02T10:55:24.847	5.14×10^{-4}	1.03×10^{-4}	2.90×10^{-4}	2.26×10^{-5}	(32)	
2016-03-02T17:09:11.164	5.38×10^{-4}	1.08×10^{-4}	3.21×10^{-4}	2.51×10^{-5}	(32)	
2016-03-03T15:28:43.534	4.63×10^{-4}	9.27×10^{-5}	3.49×10^{-4}	2.73×10^{-5}	(32)	
2016-03-04T02:36:37.079	5.03×10^{-4}	1.01×10^{-4}	4.22×10^{-4}	3.30×10^{-5}	(32)	
2016-03-04T22:24:15.604	5.16×10^{-4}	1.03×10^{-4}	6.38×10^{-4}	4.99×10^{-5}	(32)	Excluded
2016-03-05T23:51:23.672	5.05×10^{-4}	1.01×10^{-4}	3.54×10^{-4}	2.76×10^{-5}	(32)	
2016-03-06T07:44:53.859	5.35×10^{-4}	1.07×10^{-4}	3.42×10^{-4}	2.67×10^{-5}	(32)	
2016-03-06T16:55:58.808	5.55×10^{-4}	1.11×10^{-4}	5.82×10^{-4}	4.55×10^{-5}	(32)	Excluded
2016-03-06T15:17:05.287	4.91×10^{-4}	9.83×10^{-5}	5.50×10^{-4}	4.30×10^{-5}	(32)	Excluded
2016-03-07T09:13:23.939	4.54×10^{-4}	9.09×10^{-5}	4.00×10^{-4}	3.12×10^{-5}	(32)	Excluded
2016-03-07T21:06:48.488	5.35×10^{-4}	1.07×10^{-4}	3.01×10^{-4}	2.35×10^{-5}	(32)	
2016-03-08T07:09:13.447	4.80×10^{-4}	9.61×10^{-5}	3.52×10^{-4}	2.75×10^{-5}	(32)	
2016-03-08T14:40:11.610	4.80×10^{-4}	9.61×10^{-5}	5.85×10^{-4}	4.57×10^{-5}	(32)	Excluded

Date and time of measurement	Published	Error	This work	Error	Ref.	Quality note
2016-03-09T06:07:33.825	5.44×10^{-4}	1.09×10^{-4}	4.39×10^{-4}	3.43×10^{-5}	(32)	Excluded
2016-03-10T12:35:30.139	5.30×10^{-4}	1.06×10^{-4}	6.57×10^{-4}	5.13×10^{-5}	(32)	Excluded
2016-03-10T18:27:09.070	4.76×10^{-4}	9.52×10^{-5}	4.57×10^{-4}	3.57×10^{-5}	(32)	
2016-03-09T19:20:39.237	4.28×10^{-4}	8.56×10^{-5}	3.66×10^{-4}	2.86×10^{-5}	(32)	
2016-03-11T14:00:40.890	4.54×10^{-4}	9.08×10^{-5}	4.50×10^{-4}	3.52×10^{-5}	(32)	
2016-03-12T15:34:53.179	4.89×10^{-4}	9.77×10^{-5}	2.36×10^{-4}	1.84×10^{-5}	(32)	
2016-03-11T22:24:59.212	5.30×10^{-4}	1.06×10^{-4}	3.71×10^{-4}	2.90×10^{-5}	(32)	
2016-03-12T15:34:53.179	5.30×10^{-4}	1.06×10^{-4}	2.36×10^{-4}	1.84×10^{-5}	(32)	
2016-03-12T22:24:51.847	5.37×10^{-4}	1.07×10^{-4}	3.03×10^{-4}	2.36×10^{-5}	(32)	
2016-03-13T00:34:18.741	4.80×10^{-4}	9.60×10^{-5}	3.21×10^{-4}	2.51×10^{-5}	(32)	
2016-03-13T11:42:48.733	5.17×10^{-4}	1.03×10^{-4}	4.19×10^{-4}	3.28×10^{-5}	(32)	
2016-03-13T20:41:54.171	5.19×10^{-4}	1.04×10^{-4}	5.34×10^{-4}	4.17×10^{-5}	(32)	Excluded
2016-03-14T03:51:16.292	4.58×10^{-4}	9.16×10^{-5}	3.98×10^{-4}	3.11×10^{-5}	(32)	
2016-03-14T16:48:37.968	4.80×10^{-4}	9.60×10^{-5}	3.78×10^{-4}	2.96×10^{-5}	(32)	
2016-03-14T19:42:02.680	4.49×10^{-4}	8.98×10^{-5}	6.97×10^{-4}	5.44×10^{-5}	(32)	Excluded
2016-03-15T22:13:58.818	4.71×10^{-4}	9.42×10^{-5}	4.58×10^{-4}	3.58×10^{-5}	(32)	Excluded
2016-03-16T17:53:00.031	4.53×10^{-4}	9.07×10^{-5}	4.43×10^{-4}	3.46×10^{-5}	(32)	
2016-03-17T23:04:44.733	4.71×10^{-4}	9.42×10^{-5}	3.33×10^{-4}	2.60×10^{-5}	(32)	
2016-03-18T08:58:23.509	5.43×10^{-4}	1.09×10^{-4}	4.74×10^{-4}	3.70×10^{-5}	(32)	Excluded
2016-03-18T19:31:59.544	5.60×10^{-4}	1.12×10^{-4}	3.83×10^{-4}	2.99×10^{-5}	(32)	
2016-03-19T23:08:26.799	5.06×10^{-4}	1.01×10^{-4}	3.84×10^{-3}	3.00×10^{-4}	(32)	Excluded
2016-03-21T01:04:12.620	5.62×10^{-4}	1.12×10^{-4}	4.47×10^{-4}	3.49×10^{-5}	(32)	
2016-03-21T10:40:08.141	5.25×10^{-4}	1.05×10^{-4}	4.11×10^{-4}	3.21×10^{-5}	(32)	Excluded
2016-03-21T17:29:47.010	4.86×10^{-4}	9.71×10^{-5}	4.43×10^{-4}	3.46×10^{-5}	(32)	Excluded
2016-03-22T02:52:01.201	4.49×10^{-4}	8.97×10^{-5}	4.35×10^{-4}	3.40×10^{-5}	(32)	
2016-03-22T14:41:36.841	5.29×10^{-4}	1.06×10^{-4}	4.23×10^{-4}	3.31×10^{-5}	(32)	
2016-03-15T04:19:59.841	5.70×10^{-4}	1.14×10^{-4}	4.21×10^{-4}	3.29×10^{-5}	(34)	
2016-03-15T05:03:15.333	5.13×10^{-4}	1.03×10^{-4}	6.00×10^{-4}	4.69×10^{-5}	(34)	Excluded
2016-03-15T19:11:45.817	4.02×10^{-4}	8.04×10^{-5}	3.46×10^{-4}	2.70×10^{-5}	(34)	
2016-03-15T00:41:09.901	5.40×10^{-4}	1.08×10^{-4}	6.94×10^{-4}	5.42×10^{-5}	(34)	Excluded
2016-03-15T21:30:53.149	5.74×10^{-4}	1.15×10^{-4}	3.90×10^{-4}	3.04×10^{-5}	(34)	Excluded
2016-03-16T07:14:35.098	7.00×10^{-4}	1.40×10^{-4}	4.10×10^{-4}	3.20×10^{-5}	(34)	Excluded
2016-03-16T07:58:33.113	5.68×10^{-4}	1.14×10^{-4}	4.34×10^{-4}	3.39×10^{-5}	(34)	Excluded
2016-03-20T06:52:57.621	5.11×10^{-4}	1.02×10^{-4}	6.54×10^{-4}	5.11×10^{-5}	(34)	Excluded
2016-03-21T02:58:29.225	4.90×10^{-4}	9.80×10^{-5}	5.19×10^{-4}	4.05×10^{-5}	(34)	
2016-03-21T03:50:27.260	5.02×10^{-4}	1.00×10^{-4}	6.74×10^{-4}	5.27×10^{-5}	(34)	Excluded
2016-03-21T04:33:42.808	6.18×10^{-4}	1.24×10^{-4}	6.57×10^{-4}	5.13×10^{-5}	(34)	Excluded

Date and time of measurement	Published	Error	This work	Error	Ref.	Quality note
2016-03-21T05:16:54.306	4.48×10^{-4}	8.96×10^{-5}	4.85×10^{-4}	3.79×10^{-5}	(34)	
2016-03-21T09:57:18.632	5.39×10^{-4}	1.08×10^{-4}	5.18×10^{-4}	4.05×10^{-5}	(34)	Excluded

Table S6.

Correlations, c , from Figure 3 of the main article. Strong correlations ($c \geq 0.5$) and anti-correlations ($c \leq -0.5$) are bolded. Weak correlations ($0.2 \leq c \leq 0.5$) and anti-correlations ($-0.5 \leq c \leq -0.2$) are italicized.

Table S7.

Average and standard deviation D/H for different time periods and comet distance constraints. The skewness indicates whether the distribution is a normal distribution or skewed positively or negatively. The number of points included in the average is given as N.

	Average D/H	Error	Std. dev.	Skewness	N
Full mission	6.16×10^{-4}	4.81×10^{-5}	5.14×10^{-4}	2.95	4339
Dust phase 1, all distances	4.25×10^{-4}	1.11×10^{-6}	2.43×10^{-4}	1.33	1185
Dust phase 2, all distances	3.75×10^{-4}	8.39×10^{-7}	9.20×10^{-5}	1.66	1290
Dust phase 3, all distances	9.05×10^{-4}	2.02×10^{-6}	6.52×10^{-4}	2.05	1864
Pre-perihelion <40 km, South	4.85×10^{-4}	2.26×10^{-6}	1.45×10^{-4}	2.42	308
Pre-perihelion <40 km, North	2.13×10^{-3}	1.51×10^{-5}	7.74×10^{-4}	0.53	138
Post-perihelion <40 km, South	3.72×10^{-4}	2.27×10^{-6}	8.43×10^{-5}	4.46	173
Post-perihelion <40 km, North	3.83×10^{-4}	2.15×10^{-6}	5.30×10^{-5}	0.60	198
Full mission <40 km	7.96×10^{-4}	2.15×10^{-6}	7.26×10^{-4}	2.10	1532
Full mission <120 km	6.87×10^{-4}	1.25×10^{-6}	5.71×10^{-4}	2.66	3131
Full mission >120 km	4.32×10^{-4}	1.11×10^{-6}	2.41×10^{-4}	1.25	1208
Pre-perihelion <120 km	9.15×10^{-4}	2.07×10^{-6}	6.58×10^{-4}	2.01	1811
Pre-perihelion >120 km	5.33×10^{-4}	1.66×10^{-6}	2.52×10^{-4}	0.69	766
Post-perihelion <120 km	3.74×10^{-4}	8.27×10^{-7}	9.14×10^{-5}	1.68	1320
Post-perihelion >120 km	2.59×10^{-4}	9.73×10^{-7}	3.63×10^{-5}	0.10	442
Previously published	5.01×10^{-4}	0.41×10^{-4}	n/a	n/a	150

Table S8.

Average, error on the mean, and standard deviation $^{16}\text{O}/^{17}\text{O}$ for different time periods and comet distance constraints. The skewness indicates whether the distribution is a normal distribution or skewed positively or negatively. The number of points included in the average is given as N.

	Average $^{16}\text{O}/^{17}\text{O}$	Error	Std. dev.	Skewness	N
Full mission	1811	142	465	0.78	4339
Dust phase 1, all distances	1885	4	439	0.48	1185
Dust phase 2, all distances	1772	4	273	1.03	1290
Dust phase 3, all distances	1790	3	569	0.76	1864
Pre-perihelion <40 km, South	2139	10	523	0.72	308
Pre-perihelion <40 km, North	1192	8	218	0.46	138
Post-perihelion <40 km, South	1776	11	244	0.55	173
Post-perihelion <40 km, North	1738	10	183	0.77	198
Full mission <40 km	1698	4	451	0.89	1532
Full mission <120 km	1784	3	472	0.91	3131
Full mission >120 km	1880	4	438	0.48	1208
Pre-perihelion <120 km	1791	3	575	0.76	1811
Pre-perihelion >120 km	1687	5	367	0.55	766
Post-perihelion <120 km	1775	4	272	1.02	1320
Post-perihelion >120 km	2214	8	340	1.51	442
Previously published	2347	191	n/a	n/a	150

Table S9.

Average and standard deviation $^{16}\text{O}/^{18}\text{O}$ for different time periods and comet distance constraints. The skewness indicates whether the distribution is a normal distribution or skewed positively or negatively. The number of points included in the average is given as N.

	Average $^{16}\text{O}/^{18}\text{O}$	Error	Std. dev.	Skewness	N
Full mission	392	32	60	0.42	9177
Dust phase 1, all distances	383	1	58	-0.33	1185
Dust phase 2, all distances	435	1	52	-0.43	1290
Dust phase 3, all distances	402	1	55	1.57	1864
Pre-perihelion <40 km, South	391	2	40	1.27	308
Pre-perihelion <40 km, North	398	3	50	0.49	138
Post-perihelion <40 km, South	436	3	62	-0.76	173
Post-perihelion <40 km, North	434	3	45	-0.50	198
Full mission <40 km	360	0	53	0.31	4025
Full mission <120 km	416	1	56	0.74	3131
Full mission >120 km	382	1	58	-0.31	1208
Pre-perihelion <120 km	403	1	54	1.68	1811
Pre-perihelion >120 km	376	1	47	-0.76	766
Post-perihelion <120 km	434	1	52	-0.40	1320
Post-perihelion >120 km	392	2	73	-0.33	442
Previously published	445	35	n/a	n/a	3820

Data S1. (separate file)

This dataset is a csv file containing the water isotope ratios, the uncertainty of each measurement, the time of the measurements, the distance from the Sun in AU, from the nucleus in km, and the subspacecraft latitude.

REFERENCES AND NOTES

1. National Academies of Sciences, Engineering, and Medicine. *Origins, Worlds, and Life: A Decadal Strategy for Planetary Science and Astrobiology 2023–2032*. (National Academies Press, Washington, DC 2022).
2. E. Jacquet, F. Robert, Water transport in protoplanetary disks and the hydrogen isotopic composition of chondrites. *Icarus* **223**, 722–732 (2013).
3. P. R. Mahaffy, T. M. Donahue, S. K. Atreya, T. C. Owen, H. B. Niemann, Galileo probe measurements of D/H and 3He/4He in Jupiter's atmosphere. *Space. Sci. Rev.* **84**, 251–263 (1998).
4. G. L. Villanueva, M. J. Mumma, R. E. Novak, H. U. Käufl, P. Hartogh, T. Encrenaz, A. Tokunaga, A. Khayat, M. D. Smith, Strong water isotopic anomalies in the martian atmosphere: Probing current and ancient reservoirs. *Science*, **348**, 218–221 (2015).
5. H. Lammer, R. Brasser, A. Johansen, M. Scherf, M. Leitzinger, Formation of Venus, Earth and Mars: Constrained by isotopes. *Space. Sci. Rev.*, **217**, 1–35 (2021).
6. P. Hartogh, D. C. Lis, D. Bockelée-Morvan, M. de Val-Borro, N. Biver, M. Küppers, M. Emprechtinger, E. A. Bergin, J. Crovisier, M. Rengel, R. Moreno, S. Szutowicz, G. A. Blake, Ocean-like water in the Jupiter-family comet 103P/Hartley 2. *Nature* **478**, 218–220 (2011).
7. B. Marty, The origins and concentrations of water, carbon, nitrogen and noble gases on Earth. *Earth Planet. Sci. Lett.* **313-314**, 56–66 (2012).
8. L. Piani, Y. Marrocchi, T. Rigaudier, L. G. Vacher, D. Thomassin, B. Marty, Earth's water may have been inherited from material similar to enstatite chondrite meteorites. *Science*, **369** 1110–1113 (2020).
9. K. Mezger, A. Maltese, H. Vollstaedt, Accretion and differentiation of early planetary bodies as recorded in the composition of the silicate Earth. *Icarus* **365**, 114497 (2021).

10. K. Altweegg, H. Balsiger, A. Bar-Nun, J. J. Berthelier, A. Bieler, P. Bochsler, C. Briois, U. Calmonte, M. Combi, J. De Keyser, P. Eberhardt, B. Fiethe, S. Fuselier, S. Gasc, T. I. Gombosi, K.C. Hansen, M. Hässig, A. Jäckel, E. Kopp, A. Korth, L. Leroy, U. Mall, B. Marty, O. Mousis, E. Neefs, T. Owen, H. Rème, M. Rubin, T. Sémon, C.-Y. Tzou, H. Waite, P. Wurz, 67P/Churyumov-Gerasimenko, a Jupiter family comet with a high D/H ratio. *Science* **347**, 1261952 (2015).
11. D.C. Lis, N. Biver, D. Bockelée-Morvan, P. Hartogh, E. A. Bergin, G. A. Blake, J. Crovisier, M. de Val-Borro, E. Jehin, M. Küppers, J. Manfroid, R. Moreno, M. Rengel, S. Szutowicz, A Herschel study of D/H in water in the Jupiter-family comet 45P/Honda-Mrkos-Pajdušáková and prospects for D/H measurements with CCAT. *Astrophys. J. Lett.* **774**, L3 (2013).
12. D. C. Lis, D. Bockelée-Morvan, R. Güsten, N. Biver, J. Stutzki, Y. Delorme, C. Durán, H. Wiesemeyer, Y. Okada, Terrestrial deuterium-to-hydrogen ratio in water in hyperactive comets. *Astron. Astrophys.* **625**, L5 (2019).
13. N. Biver, D. Bockelée-Morvan, J. Crovisier, D. C. Lis, R. Moreno, P. Colom, F. Henry, F. Herpin, G. Paubert, M. Womack, Radio wavelength molecular observations of comets C/1999 T1 (McNaught-Hartley), C/2001 A2 (LINEAR), C/2000 WM1 (LINEAR) and 153P/Ikeya-Zhang. *Astron. Astrophys.* **449**, 1255–1270 (2006).
14. E. L. Gibb, B. P. Bonev, G. Villanueva, M. A. DiSanti, M. J. Mumma, E. Sudholt, Y. Radeva, Chemical composition of Comet C/2007 N3 (Lulin): Another “atypical” comet. *Astrophys. J.* **750**, 102 (2012).
15. N. Biver, R. Moreno, D. Bockelée-Morvan, A. Sandqvist, P. Colom, J. Crovisier, D. C. Lis, J. Boissier, V. Debout, G. Paubert, S. Milam, A. Hjalmarson, S. Lundin, T. Karlsson, M. Battelino, U. Frisk, D. Murtagh; The Odin team, Isotopic ratios of H, C, N, O, and S in comets C/2012 F6 (Lemmon) and C/2014 Q2 (Lovejoy). *Astron. Astrophys.* **589**, A78 (2016).
16. L. Paganini, M.J. Mumma, E. Gibb, G.L. Villanueva, Ground-based detection of deuterated water in comet C/2014 Q2 (Lovejoy) at IR wavelengths. *Astrophys. J. Lett.* **836**, L25 (2017).

17. M. Womack, G. Sarid, K. Wierzchos, CO and other volatiles in distantly active comets. *Publ. Astron. Soc. Pac.* **129**, 031001 (2017).
18. A. Gicquel, J. B. Vincent, J. Agarwal, M. F. A'Hearn, I. Bertini, D. Bodewits, H. Sierks, Z.-Y. Lin, C. Barbieri, P. L. Lamy, R. Rodrigo, D. Koschny, H. Rickman, H. U. Keller, M. A. Barucci, J.-L. Bertaux, S. Besse, G. Cremonese, V. Da Deppo, B. Davidsson, S. Debei, J. Deller, M. De Cecco, E. Frattin, M. R. El-Maarry, S. Fornasier, M. Fulle, O. Groussin, P. J. Gutiérrez, P. Gutiérrez-Marquez, C. Güttler, S. Höfner, M. Hofmann, X. Hu, S. F. Hviid, W.-H. Ip, L. Jorda, J. Knollenberg, G. Kovacs, J.-R. Kramm, E. Kührt, M. Küppers, L. M. Lara, M. Lazzarin, J. J. Lopez Moreno, S. Lowry, F. Marzari, N. Masoumzadeh, M. Massironi, F. Moreno, S. Mottola, G. Naletto, N. Oklay, M. Pajola, A. Pommerol, F. Preusker, F. Scholten, X. Shi, N. Thomas, I. Toth, C. Tubiana, Sublimation of icy aggregates in the coma of comet 67P/Churyumov–Gerasimenko detected with the OSIRIS cameras on board Rosetta. *Mon. Not. R. Astron. Soc.* **462**, S57–S66 (2016).
19. N. Biver, D. Bockelée-Morvan, M. Hofstadter, E. Lellouch, M. Choukroun, S. Gulkis, J. Crovisier, F. P. Schloerb, L. Rezac, P. von Allmen, S. Lee, W. H. Ip, P. Hartogh, P. Encrenaz, G. Beaudin; The MIRO team, Long-term monitoring of the outgassing and composition of comet 67P/Churyumov-Gerasimenko with the Rosetta/MIRO instrument. *Astron. Astrophys.* **630**, A19 (2019).
20. H. Balsiger, P. Bochsler, P. Eberhardt, J. Fischer, S. Graf, A. Jäckel, E. Kopp, U. Langer, M. Mildner, J. Müller, T. Riesen, M. Rubin, S. Scherer, P. Wurz, S. Wüthrich, E. Arijs, S. Delanoye, J. De Keyser, E. Neefs, D. Nevejans, H. Rème, C. Aoustin, C. Mazelle, J.-L. Médale, J. A. Sauvaud, J.-J. Berthelier, J.-L. Bertaux, L. Duvet, J.-M. Illiano, S. A. Fuselier, A. G. Ghielmetti, T. Magoncelli, E. G. Shelley, A. Korth, K. Heerlein, H. Lauche, S. Livi, A. Loose, U. Mall, B. Wilken, F. Gliem, B. Fiethe, T. I. Gombosi, B. Block, G. R. Carignan, L. A. Fisk, J. H. Waite, D. T. Young, H. Wollnik, Rosina–Rosetta orbiter spectrometer for ion and neutral analysis. *Space. Sci. Rev.* **128**, 745–801 (2007).

21. B. Pestoni, K. Altwegg, H. Balsiger, N. Hänni, M. Rubin, I. Schroeder, M. Schuhmann, S. Wampfler. Detection of volatiles undergoing sublimation from 67P/Churyumov-Gerasimenko coma particles using ROSINA/COPS-II. The nude gauge. *Astron. Astrophys.*, **651**, A26 (2021).
22. J. de Keyser, F. Dhooghe, K. Altwegg, H. Balsiger, J.-J. Berthelier, C. Briois, U. Calmonte, G. Cessateur, M. R. Combi, E. Equeter, B. Fiethe, S. Fuselier, S. Gasc, A. Gibbons, T. Gombosi, H. Gunell, M. Hässig, L. Le Roy, R. Maggiolo, U. Mall, B. Marty, E. Neefs, H. Rème, M. Rubin, T. Sémond, C.-Y. Tzou, P. Wurz, Evidence for distributed gas sources of hydrogen halides in the coma of comet 67P/Churyumov–Gerasimenko. *Mon. Not. R. Astron. Soc.* **469**, S695–S711 (2017).
23. M. Hoang, P. Garnier, J. Lasue, H. Rème, M. T. Capria, K. Altwegg, M. Läuter, T. Kramer, M. Rubin, Investigating the Rosetta/RTOF observations of comet 67P/Churyumov-Gerasimenko using a comet nucleus model: Influence of dust mantle and trapped CO. *Astron. Astrophys.* **638**, A106 (2020).
24. G. A. Blake, C. Qi, M. R. Hogerheijde, M. A. Gurwell, D. O. Muhleman, Sublimation from icy jets as a probe of the interstellar volatile content of comets. *Nature* **398**, 213–216 (1999).
25. R. H. Brown, D. S. Lauretta, B. Schmidt, J. Moores, Experimental and theoretical simulations of ice sublimation with implications for the chemical, isotopic, and physical evolution of icy objects. *Planet. Space Sci.* **60**, 166–180 (2012).
26. C. Lécuyer, A. Royer, F. Fourel, M. Seris, L. Simon, F. Robert. D/H fractionation during the sublimation of water ice. *Icarus*, **285**, 1–7 (2017).
27. J. E. Moores, R. H. Brown, D. S. Lauretta, P. H. Smith. Experimental and theoretical simulation of sublimating dusty water ice with implications for D/H ratios of water ice on Comets and Mars. *Planet. Sci.* **1**, 2 (2012).
28. B.J. Davidsson, S. Birch, G. A. Blake, D. Bodewits, J. P. Dworkin, D. P. Glavin, Y. Furukawa, J. I. Lunine, J. L. Mitchell, A. N. Nguyen, S. Squyres, A. Takigawa, J.-B. Vincent, K. Zacny, Airfall on comet 67P/Churyumov–Gerasimenko. *Icarus* **354**, 114004 (2021).

29. S. Fornasier, S. Mottola, H.U. Keller, M. A. Barucci, B. Davidsson, C. Feller, J. D. P. Deshapriya, H. Sierks, C. Barbieri, P. L. Lamy, R. Rodrigo, D. Koschny, H. Rickman, M. A'Hearn, J. Agarwal, J.-L. Bertaux, I. Bertini, S. Besse, G. Cremonese, V. Da Deppo, S. Debei, M. De Cecco, J. Deller, M. R. El-Maarry, M. Fulle, O. Groussin, P. J. Gutierrez, C. Güttler, M. Hofmann, S. F. Hviid, W.-H. Ip, L. Jorda, J. Knollenberg, G. Kovacs, R. Kramm, E. Kührt, M. Küppers, M. L. Lara, M. Lazzarin, J. J. Lopez Moreno, F. Marzari, M. Massironi, G. Naletto, N. Oklay, M. Pajola, A. Pommerol, F. Preusker, F. Scholten, X. Shi, N. Thomas, I. Toth, C. Tubiana, J.-B. Vincent, Rosetta's comet 67P/Churyumov-Gerasimenko sheds its dusty mantle to reveal its icy nature. *Science* **354**, 1566–1570 (2016).
30. M. Choukroun, K. Altwegg, E. Kührt, N. Biver, D. Bockelée-Morvan, J. Drążkowska, A. Hérique, M. Hilchenbach, R. Marschall, M. Pätzold, M. G. T. Taylor, N. Thomas, Dust-to-gas and refractory-to-ice mass ratios of comet 67P/Churyumov-Gerasimenko from Rosetta observations. *Space. Sci. Rev.* **216**, 44 (2020).
31. H.U. Keller, S. Mottola, S. Hviid, J. Agarwal, E. Kührt, Y. Skorov, K. Otto, J.-B. Vincent, N. Oklay, S. E. Schröder, B. Davidsson, M. Pajola, X. Shi, D. Bodewits, I. Toth, F. Preusker, F. Scholten, H. Sierks, C. Barbieri, P. Lamy, R. Rodrigo, D. Koschny, H. Rickman, M. F. A'Hearn, M. A. Barucci, J.-L. Bertaux, I. Bertini, G. Cremonese, V. Da Deppo, S. Debei, M. De Cecco, J. Deller, S. Fornasier, M. Fulle, O. Groussin, P. J. Gutierrez, C. Güttler, M. Hofmann, W.-H. Ip, L. Jorda, J. Knollenberg, J. R. Kramm, M. Küppers, L.-M. Lara, M. Lazzarin, J. J. Lopez-Moreno, F. Marzari, G. Naletto, C. Tubiana, N. Thomas, Seasonal mass transfer on the nucleus of comet 67P/Churyumov–Gerasimenko. *Mon. Not. R. Astron. Soc.*, **469**, S357–S371 (2017).
32. D. R. Müller, K. Altwegg, J. J. Berthelier, M. Combi, J. De Keyser, S. A. Fuselier, N. Hänni, B. Pestoni, M. Rubin, I. R. Schroeder, S. F. Wampfler High D/H ratios in water and alkanes in comet 67P/Churyumov-Gerasimenko measured with Rosetta/ROSINA DFMS. *Astron. Astrophys.* **662**, A69 (2022).
33. I. R. Schroeder, K. Altwegg, H. Balsiger, J.-J. Berthelier, M. R. Combi, J. De Keyser, B. Fiethe, S. A. Fuselier, T. I. Gombosi, K. C. Hansen, M. Rubin, Y. Shou, V. M. Tenishev, T. Sémon, S. F. Wampfler, P. Wurz, A comparison between the two lobes of comet 67P/Churyumov–

Gerasimenko based on D/H ratios in H₂O measured with the Rosetta/ROSINA DFMS. *Mon. Not. R. Astron. Soc.* **489**, 4734–4740 (2019).

34. K. Altwegg, H. Balsiger, J. Berthelier, A. Bieler, U. Calmonte, J. De Keyser, B. Fiethe, S. A. Fuselier, S. Gasc, T. I. Gombosi, T. Owen, L. Le Roy, M. Rubin, T. Sémon, C.-Y. Tzou. D₂O and HDS in the coma of 67P/Churyumov–Gerasimenko. *Philos. Trans. A Math. Phys. Eng. Sci.* **375**, 20160253 (2017).
35. M. Hässig, K. Altwegg, H. Balsiger, J.-J. Berthelier, U. Calmonte, M. Combi, J. De Keyser, B. Fiethe, S. A. Fuselier, M. Rubin, ROSINA/DFMS capabilities to measure isotopic ratios in water at comet 67P/Churyumov–Gerasimenko. *Planet. Space Sci.* **84**, 148–152 (2013).
36. I. R. Schroeder, K. Altwegg, H. Balsiger, J.-J. Berthelier, J. De Keyser, B. Fiethe, S. A. Fuselier, S. Gasc, T. I. Gombosi, M. Rubin, T. Sémon, C.-Y. Tzou, S. F. Wampfler, P. Wurz. ¹⁶O/¹⁸O ratio in water in the coma of comet 67P/Churyumov-Gerasimenko measured with the Rosetta/ROSINA double-focusing mass spectrometer. *Astron. Astrophys.* **630**, A29 (2019).
37. A. Luspay-Kuti, K. Altwegg, J. J. Berthelier, A. Beth, F. Dhooghe, B. Fiethe, S. A. Fuselier, T. I. Gombosi, K. C. Hansen, M. Hässig, G. Livadiotis, U. Mall, K. E. Mandt, O. Mousis, S. M. Petrinec, M. Rubin, K. J. Trattner, C.-Y. Tzou, P. Wurz, Comparison of neutral outgassing of comet 67P/Churyumov-Gerasimenko inbound and outbound beyond 3 AU from ROSINA/DFMS. *Astron. Astrophys.* **630**, A30 (2019).
38. N. Biver, D. Bockelée-Morvan, M. Hofstadter, E. Lellouch, M. Choukroun, S. Gulkis, J. Crovisier, F. P. Schloerb, L. Rezac, P. Von Allmen, S. Lee, C. Leyrat, W. H. Ip, P. Hartogh, P. Encrenaz, G. Beaudin; The MIRO team, Long-term monitoring of the outgassing and composition of comet 67P/Churyumov-Gerasimenko with the Rosetta/MIRO instrument. *Astron. Astrophys.* **630**, A19 (2019).
39. A. L. Cochran, A. J. McKay. Strong CO⁺ and N₂⁺ emission in comet C/2016 R2 (Pan-STARRS). *Astrophys. J. Lett.* **854**, L10 (2018).

40. C. Opitom, D. Hutsemekers, E. Jehin, P. Rousselot, F. J. Pozuelos, J. Manfroid, Y. Moulane, M. Gillon, Z. Benkhaldoun. High resolution optical spectroscopy of the N₂-rich comet C/2016 R2 (PanSTARRS). *Astron. Astrophys.* **624**, A64 (2019).
41. J. J. Kavelaars, O. Mousis, J.-M. Petit, H. A. Weaver, On the formation location of Uranus and Neptune as constrained by dynamical and chemical models of comets. *Astrophys. J. Lett.* **734**, L30, (2011).
42. J. H. Waite, W. S. Lewis, B. A. Magee, J. I. Lunine, W. B. McKinnon, C. R. Glein, O. Mousis, D. T. Young, T. Brockwell, J. Westlake, M.-J. Nguyen, B. D. Teolis, H. B. Niemann, R. L. McNutt Jr, M. Perry, W.-H. Ip, Liquid water on Enceladus from observations of ammonia and 40Ar in the plume. *Nature* **460**, 487–490 (2009).
43. R. N. Clark, R. H. Brown, D. P. Cruikshank, G. A. Swayze, Isotopic ratios of Saturn's rings and satellites: Implications for the origin of water and Phoebe. *Icarus* **321**, 791–802 (2019).
44. C. Ceccarelli, P. Caselli, D. Bockelée-Morvan, O. Mousis, S. Pizzarello, F. Robert, D. Semenov. “Deuterium fractionation: The Ariadne's thread from the precollapse phase to meteorites and comets today” in *Protostars and Planets VI*, (The University of Arizona Space Science Series, 2014), p. 859–882.
45. A. Luspay-Kuti, O. Mousis, M. Hässig, S. A. Fuselier, J. I. Lunine, B. Marty, K. E. Mandt, Peter Wurz, Martin Rubin, The presence of clathrates in comet 67P/Churyumov-Gerasimenko. *Sci. Adv.* **2**, e1501781 (2016).
46. O. Mousis, J.I. Lunine, A. Luspay-Kuti, T. Guillot, B. Marty, M. Ali-Dib, P. Wurz, K. Altwegg, A. Bieler, M. Hässig, M. Rubin, P. Vernazza, J. H. Waite, A protosolar nebula origin for the ices agglomerated by comet 67P/Churyumov–Gerasimenko. *Astrophys. J. Lett.*, **819** L33 (2016).
47. O. Mousis, T. Ronnet, J. I. Lunine, A. Luspay-Kuti, K. E. Mandt, G. Danger, F. Pauzat, Y. Ellinger, P. Wurz, P. Vernazza, L. Le Sergeant d'Hendecourt. Noble gas abundance ratios indicate the agglomeration of 67P/Churyumov–Gerasimenko from warmed-up ice. *Astrophys. J. Lett.* **865**, L11 (2018).

48. E. G. Johnson, A. O. Nier. Angular aberrations in sector shaped electromagnetic lenses for focusing beams of charged particles. *Phys. Rev.* **91**, 10 (1953).
49. J. De Keyser, A. Gibbons, F. Dhooghe, K. Altwegg, H. Balsiger, J.-J. Berthelier, S. A. Fuselier, T. I. Gombosi, E. Neefs, M. Rubin, Calibration of parent and fragment ion detection rates in Rosettas ROSINA/DFMS mass spectrometer. *Int. J. Mass Spectrom.* **446**, 116233 (2019).
50. M.M. Hässig. *Sensitivity and fragmentation calibration of the ROSINA double focusing mass spectrometer* (University of Bern, 2013).
51. J. Skilling. Nested sampling. In *AIP Conf. Proc.*, **735**, p. 395–405. American Institute of Physics (2004).
52. J. S. Speagle, DYNESTY: A dynamic nested sampling package for estimating Bayesian posteriors and evidences. *Mon. Not. R. Astron. Soc.* **493**, 3132–3158 (2020).
53. F. Feroz, M. P. Hobson, Multimodal nested sampling: An efficient and robust alternative to Markov Chain Monte Carlo methods for astronomical data analyses. *Mon. Not. R. Astron. Soc.*, **384**, 449–463 (2008).
54. K. Lodders. Relative atomic solar system abundances, mass fractions, and atomic masses of the elements and their isotopes, composition of the solar photosphere, and compositions of the major chondritic meteorite groups. *Space. Sci. Rev.* **217**, 44 (2021).
55. E. Lellouch, B. Bézard, T. Fouchet, H. Feuchtgruber, T. Encrenaz, T. de Graauw, The deuterium abundance in Jupiter and Saturn from ISO-SWS observations. *Astron. Astrophys.* **370**, 610–622 (2001).
56. O. Mousis, D. H. Atkinson, R. Ambrosi, S. Atreya, D. Banfield, S. Barabash, M. Blanc, T. Cavalié, A. Coustenis, M. Deleuil, G. Durry, F. Ferri, L. N. Fletcher, T. Fouchet, T. Guillot, P. Hartogh, R. Hueso, M. Hofstadter, J.-P. Lebreton, K. E. Mandt, H. Rauer, P. Rannou, J.-B. Renard, A. Sánchez-Lavega, K. M. Sayanagi, A. A. Simon, T. Spilker, E. Venkatapathy, J. H. Waite, P. Wurz, In situ exploration of the giant planets. *Exp. Astron.* **54**, 975–1031 (2022).

57. H. Feuchtgruber, E. Lellouch, G. Orton, T. de Graauw, B. Vandenbussche, B. Swinyard, R. Moreno, C. Jarchow, F. Billebaud, T. Cavalie, S. Sidher, P. Hartogh. The D/H ratio in the atmospheres of Uranus and Neptune from Herschel-PACS observations. *Astron. Astrophys.*, **551**, A126 (2013).
58. K. S. Noll, T. R. Geballe, R. F. Knacke. Detection of H₂18O in Jupiter. *Astrophys. J.*, **453**, L49–L53 (1995).
59. C. M. O'D. Alexander, R. Bowden, M. L. Fogel, K. T. Howard, C. D. K. Herd, L. R. Nittler, The provenances of asteroids, and their contributions to the volatile inventories of the terrestrial planets. *Science*, **337**, 721–723 (2012).
60. C.M.O'D. Alexander, Quantitative models for the elemental and isotopic fractionations in chondrites: The carbonaceous chondrites. *Geochim. Cosmochim. Acta* **254**, 277–309 (2019).
61. C.M.O.D. Alexander, Quantitative models for the elemental and isotopic fractionations in the chondrites: The non-carbonaceous chondrites. *Geochim. Cosmochim. Acta* **254**, 246–276 (2019).
62. K. Altwegg, H. Balsiger, M. Combi, J. De Keyser, M. N. Drozdovskaya, S. A. Fuselier, T. I. Gombosi, N. Hänni, M. Rubin, M. Schuhmann, I. Schroeder, S. Wampfler, Molecule-dependent oxygen isotopic ratios in the coma of comet 67P/Churyumov–Gerasimenko. *Mon. Not. R. Astron. Soc.* **498**, 5855–5862 (2020).
63. J. A. Paquette, C. Engrand, M. Hilchenbach, N. Fray, O. J. Stenzel, J. Silen, J. Rynö, J. Kissel; The Cosima Team, The oxygen isotopic composition (¹⁸O/¹⁶O) in the dust of comet 67P/Churyumov-Gerasimenko measured by COSIMA on-board Rosetta. *Mon. Not. R. Astron. Soc.* **477**, 3836–3844 (2018).
64. M. Hässig, K. Altwegg, H. Balsiger, J. J. Berthelier, A. Bieler, U. Calmonte, F. Dhooghe, B. Fiethe, S. A. Fuselier, S. Gasc, T. I. Gombosi, L. Le Roy, A. Luspay-Kuti, K. Mandt, M. Rubin, C.-Y. Tzou, S. F. Wampfler, P. Wurz, Isotopic composition of CO₂ in the coma of 67P/Churyumov-Gerasimenko measured with ROSINA/DFMS. *Astron. Astrophys.* **605**, A50 (2017).

65. K. E. Mandt, J. H. Waite, W. Lewis, B. Magee, J. Bell, J. Lunine, O. Mousis, D. Cordier, Isotopic evolution of the major constituents of Titan's atmosphere based on Cassini data. *Planet. Space Sci.* **57**, 1917–1930 (2009).
66. K. E. Mandt, J. H. Waite, B. Teolis, B. A. Magee, J. Bell, J. H. Westlake, C. A. Nixon, O. Mousis, J. I. Lunine, The $^{12}\text{C}/^{13}\text{C}$ ratio on Titan from Cassini INMS measurements and implications for the evolution of methane. *Astrophys. J.* **749**, 160 (2012).
67. J. Serigano, C. A. Nixon, M.A. Cordiner, P. G. J. Irwin, N. A. Teanby, S. B. Charnley, J. E. Lindberg, Isotopic ratios of carbon and oxygen in Titan's CO using ALMA. *Astrophys. J. Lett.* **821**, L8 (2016).
68. W. M. Grundy, I. Wong, C. R. Glein, S. Protopapa, B. J. Holler, J. C. Cook, J. A. Stansberry, J. I. Lunine, A. H. Parker, H. B. Hammel, S. N. Milam, R. Brunetto, N. Pinilla-Alonso, A. C. de Souza Feliciano, J. P. Emery, J. Licandro, Measurement of D/H and $^{13}\text{C}/^{12}\text{C}$ ratios in methane ice on Eris and Makemake: Evidence for internal activity. *Icarus* **411**, 115923 (2024).
69. J. Murthy, R.C. Henry, H.W. Moos, W. B. Landsman, J. L. Linsky, A. Vidal-Madjar, C. Gry, IUE observations of hydrogen and deuterium in the local interstellar medium. *Adv. Space Res.* **315**, 675–686 (1987).
70. T. M. Donahue, J. H. Hoffman, R. R. Hodges, A. J. Watson, Venus was wet: A measurement of the ratio of deuterium to hydrogen. *Science*, **216**, 630–633 (1982).
71. C. R. Webster, P. R. Mahaffy, G. J. Flesch, P. B. Niles, J. H. Jones, L. A. Leshin, S. K. Atreya, J. C. Stern, L. E. Christensen, T. Owen, H. Franz, R. O. Pepin, A. Steele; The MSL Science Team, Isotope ratios of H, C, and O in CO_2 and H_2O of the Martian atmosphere. *Science* **341**, 260–263 (2013).
72. C. A. Nixon, B. Temelso, S. Vinatier, N. A. Teanby, B. Bézard, R. K. Achterberg, K. E. Mandt, C. D. Sherrill, P. G. J. Irwin, D. E. Jennings, P. N. Romani, A. Coustenis, and F. M. Flasar, Isotopic ratios in Titan's methane: Measurements and modeling. *Astrophys. J.* **749**, 159 (2012).

73. H. Balsiger, K. Altwegg, J. Geiss, D/H and $^{18}\text{O}/^{16}\text{O}$ ratio in the hydronium ion and in neutral water from in situ ion measurements in comet Halley. *J. Geophys. Res. Space Phys.* **100**, 5827–5834 (1995).
74. P. Eberhardt, M. Reber, D. Krankowsky, R. Hodges, The D/H and $^{18}\text{O}/^{16}\text{O}$ ratios in water from comet P/Halley. *Astron. Astrophys.* **302**, 301–316 (1995).
75. D. Bockelée-Morvan, D. Gautier, D. C. Lis, K. Young, J. Keene, T. Phillips, T. Owen, J. Crovisier, P. F. Goldsmith, E. A. Bergin, D. Despois, A. Wootten, Deuterated water in comet C/1996 B2 (Hyakutake) and its implications for the origin of comets. *Icarus* **133**, 147–162 (1998).
76. R. Meier, T. C. Owen, H. E. Matthews, D. C. Jewitt, D. Bockelée-Morvan, N. Biver, J. Crovisier, D. Gautier, A determination of the HDO/H₂O ratio in comet C/1995 O1 (Hale-Bopp). *Science* **279**, 842–844 (1998).
77. G. L. Villanueva, M. J. Mumma, B. P. Bonev, M. A. DiSanti, E. L. Gibb, H. Böhnhardt, M. Lippi. A sensitive search for deuterated water in comet 8P/Tuttle. *Astrophys. J.*, **690**, L5 (2009).
78. D. Bockelée-Morvan, N. Biver, B. Swinyard, M. de Val-Borro, J. Crovisier, P. Hartogh, D. C. Lis, R. Moreno, S. Szutowicz, E. Lellouch, M. Emprechtinger, G. A. Blake, R. Courtin, C. Jarchow, M. Kidger, M. Küppers, M. Rengel, G. R. Davis, T. Fulton, D. Naylor, S. Sidher, H. Walker, Herschel measurements of the D/H and $^{16}\text{O}/^{18}\text{O}$ ratios in water in the Oort-cloud comet C/2009 P1 (Garradd). *Astron. Astrophys.* **544**, L15 (2012).
79. D. Hutsemekers, J. Manfroid, E. Jehin, J. M. Zucconi, C. Arpigny, The $^{16}\text{OH}/^{18}\text{OH}$ and OD/OH isotope ratios in comet C/2002 T7 (LINEAR). *Astron. Astrophys.* **490**, L31-L34 (2008).
80. H. A. Weaver, M. F. A'Hearn C. Arpigny M. R. Combi P. D. Feldman, G.-P Tozzi, N. Dello Russo, M. C. Festou Atomic deuterium emission and the D/H ratio in comets in *Asteroids, Comets, and Meteors* (Baltimore, MD) *LPI Contrib.* **1405**, 8216 (2008).

81. J. H. Hoffman, R. R. Hodges, T. M. Donahue, M. B. McElroy. Composition of the Venus lower atmosphere from the Pioneer Venus mass spectrometer. *J. Geophys. Res. Space Phys.* **85**, 7882–7890 (1980).